

1 **Article type:** Review

2 **Prediction of oncogene mutation status in non-small cell lung cancer: A**
3 **systematic review and meta-analysis with a special focus on artificial-**
4 **intelligence-based methods**

5

6 Almudena Fuster-Matanzo^{†1}, Alfonso Picó Peris^{†1}, Fuensanta Bellvís Bataller¹, Ana
7 Jimenez-Pastor¹, Glen J. Weiss², Luis Martí-Bonmati^{3,4}, Antonio Lázaro Sánchez⁵,
8 Giuseppe L. Banna⁶, Alfredo Addeo⁷, Ángel Alberich-Bayarri¹

9

10 ¹Quantitative Imaging Biomarkers in Medicine (Quibim), 46021 Valencia, Spain

11 ²Quantitative Imaging Biomarkers in Medicine, Quibim, Boston, MA, USA, Boston,
12 MA

13 ³Grupo de Investigación Biomédica en Imagen, Instituto de Investigación Sanitaria La
14 Fe, Avenida Fernando Abril Martorell, 106 Torre A planta 7, 46026, Valencia, Spain.

15 ⁴Área Clínica de Imagen Médica, Área Clínica de Imagen Médica, Hospital Universitari
16 i Politècnic La Fe, Avinguda Fernando Abril Martorell, 106 Torre E planta 0, 46026,
17 València, Spain.

18 ⁵

19 ⁶Department of Oncology, Portsmouth Hospitals University NHS Trust, Portsmouth,
20 PO6 3LY, UK; Faculty of Science and Health, School of Pharmacy and Biomedical
21 Sciences, University of Portsmouth, Portsmouth, PO1 2UP, UK

22 ⁷University Hospital Geneva, Geneva, Switzerland.

23 [†]These authors contributed equally to this work.

24

25 **Correspondence:**

26 Almudena Fuster-Matanzo

27 Quantitative Imaging Biomarkers in Medicine (Quibim),

28 EDIFICIO EUROPA, Av. d'Aragó, 30, Planta 13

29 46021 Valencia, Spain

30 Mail: almudenafter@quibim.com

31 Tel: +34 652124031

32

33 **ABSTRACT**

34 **Background**

35 In non-small cell lung cancer (NSCLC), alternative strategies to determine patient
36 oncogene mutation status are essential to overcome some of the drawbacks associated
37 with current methods. We aimed to review the use of radiomics alone or in combination
38 with clinical data and to evaluate the performance of artificial intelligence (AI)-based
39 models on the prediction of oncogene mutation status.

40 **Methods**

41 A PRISMA-compliant literature review was conducted. The Medline (via Pubmed),
42 Embase, and Cochrane Library databases were searched for studies published through
43 June 30, 2023 predicting oncogene mutation status in patients with NSCLC using
44 radiomics. Independent meta-analyses evaluating the performance of AI-based models
45 developed with radiomics features or with a combination of radiomics features plus
46 clinical data for the prediction of different oncogenic driver mutations were performed.
47 A meta-regression to analyze the influence of methodological/clinical factors was also
48 conducted.

49 **Results**

50 Out of the 615 studies identified, 89 evaluating models for the prediction of epidermal
51 growth factor-1 (EGFR), anaplastic lymphoma kinase (ALK), and Kirsten rat sarcoma
52 virus (KRAS) mutations were included in the systematic review. A total of 38 met the
53 inclusion criteria for the meta-analyses. The AI algorithms' sensitivity/false positive rate
54 (FPR) in predicting EGFR, ALK, and KRAS mutations using radiomics-based models
55 was 0.753 (95% CI 0.721–0.783)/0.346 (95% CI 0.305–0.390), 0.754 (95% CI 0.639–
56 0.841)/ 0.225 (95% CI 0.163–0.302), and 0.744 (95% CI 0.605–0.846)/0.376 (95% CI
57 0.274–0.491), respectively. A meta-analysis of combined models was only possible for
58 EGFR mutation, revealing a sensitivity/FPR of 0.800 (95% CI 0.767–0.830)/0.335
59 (95% CI 0.279–0.396). No statistically significant results were obtained in the meta-
60 regression.

61 **Conclusions**

62 Radiomics-based models may represent valuable non-invasive tools for the
63 determination of oncogene mutation status in NSCLC. Further investigation is required
64 to analyze whether clinical data might boost their performance.

65 **Keywords:** radiomics, artificial intelligence, medical imaging, oncogene mutation
66 status, non-small cell lung cancer.

67

68 INTRODUCTION

69 Lung cancer represents the most often diagnosed cancer in both women and men
70 worldwide, ranking first and third, respectively, and remaining the leading cause of
71 cancer death¹. Non-small cell lung cancer (NSCLC), the most frequent histological
72 subtype, accounts for 80%–85% of cases, being adenocarcinoma the most common
73 subtype (40%–50% of cases). Adenocarcinoma can be further subdivided into distinct
74 molecular subtypes². Indeed, molecular subtyping has become highly relevant in the
75 disease context, as genotype-driven therapy (“targeted therapy”) is nowadays the
76 standard of care for a significant subgroup of patients with advanced and metastatic
77 NSCLC³. However, traditional methods for determining the molecular genotype, as well
78 as the possible emergence of drug resistance mutations during patient’s follow-up, entail
79 invasive biopsies and genetic sequence testing, procedures with multiple number of
80 associated drawbacks including high costs, sampling bias, lack of enough sample,
81 turnaround time, and medical complications⁴⁻⁶. Importantly, the overall accessibility of
82 molecular diagnostics and liquid biopsy may be limited for many patients⁷, highlighting
83 the need to investigate complementary methods to characterize the oncogene mutation
84 status of lesions.

85 Radiological imaging represents a potent non-invasive tool for lung cancer, from the
86 screening, diagnosis and staging of the disease to the management, therapeutic
87 planification and follow-up of both early- and advanced-stage cases⁸. Specifically,
88 computed tomography (CT) remains the standard of care for lung cancer visualization,
89 providing excellent morphological and textural information. In recent years, radiomics,
90 the process of extracting and analyzing quantitative features from medical images to
91 investigate potential connections with biology and clinical outcomes, has gained
92 increasing attention for its applicability in several oncological diseases including lung
93 cancer⁸. The application of artificial intelligence (AI) to imaging analyses has enabled
94 important clinical needs to be met. This includes the prognostication of outcomes or the
95 prediction of response to treatment, disease progression, or the mutational and
96 molecular profiling of tumors⁹. In particular, the use of radiomics coupled with AI
97 methods has demonstrated to be a promising non-invasive alternative tool for the
98 prediction of oncogene mutation status in NSCLC⁸.

99 In this systematic review and meta-analysis we aimed to: 1) review the available
100 scientific evidence on the use of imaging-based models and radiomics for the prediction

101 of the main targetable oncogenic driver alterations in NSCLC, including epidermal
102 growth factor receptor (EGFR), anaplastic lymphoma kinase (ALK), and Kirsten rat
103 sarcoma virus (KRAS); 2) analyze the overall performance of specifically, AI-based
104 methods, for the prediction of oncogene mutation status; 3) evaluate whether the
105 inclusion of clinical variables in the models improve their performance; 4) evaluate the
106 impact of the available evidence from a clinical perspective.

107 **MATERIAL AND METHODS**

108 This systematic review was conducted in accordance with the Preferred Reporting Items
109 for Systematic Reviews and Meta-Analysis (PRISMA) guidelines¹⁰. The review was
110 registered on PROSPERO before initiation (registration no. CRD42022349809).

111 **Search strategy**

112 A systematic search for eligible publications published through 30 June 2023 was per-
113 formed in Medline (via Pubmed), Cochrane Library and EMBASE databases using the
114 keywords “Radiomics”, “NSCLC” and “Mutational status”. Further details on the
115 search terms used in each database are provided in **Supplementary Table S1**. There
116 were no limitations on the publishing year, participant age, or nationality. The search
117 was exclusively limited to English-language publications.

118 **Study selection**

119 Literature search and study selection were independently performed by two reviewers
120 (A.F.M. and A.L.S.). To find relevant publications, they reviewed the titles and
121 abstracts. Studies that satisfied the inclusion criteria were then manually assessed for
122 eligibility by full-text screening. Covidence systematic review software (Veritas Health
123 Innovation, Melbourne, Australia. Available at www.covidence.org) was used as a
124 screening and data extraction tool.

125 *Inclusion criteria*

126 Papers were included in the qualitative synthesis (systematic review) if meeting the
127 following inclusion criteria based on Patient, Index test, Comparator, Reference test,
128 Diagnosis of reference (PIRD) questions: 1) being focused on the ability of radiomics to
129 predict oncogene mutation status in NSCLC; 2) radiomics features were extracted from
130 CT or from F-18 fluoro-deoxy-glucose (FDG)/CT scans; 3) a full text was available; 4)
131 were written in English.

132 *Exclusion criteria*

133 Papers describing studies conducted using MRI scans (not the standard of care for
134 NSCLC patients) or performed in phantom or animal models, or published as case
135 reports, editorials, reviews, poster presentations, letters, editorials, or meeting abstracts
136 were excluded. Papers not on the field of interest were also excluded.

137 For the quantitative synthesis (meta-analysis), the following additional exclusion
138 criteria were applied: 1) oncogene mutation status was not the primary objective of the
139 paper; 2) were focused on specific mutation subtypes; 3) did not apply AI-based
140 methodologies; 4) developed simultaneous detection models or discriminant models; 5)
141 sensitivity or specificity metrics were not available and could not be calculated; 6) were
142 not comparable with the other articles included (model was developed based on intra-
143 and extra-tumor derived radiomics features); 7) only included models developed with a
144 combination of quantitative features extracted from PET/CT or from PET images
145 (strictly adhering to a clinical perspective, PET scanning equipment is not always
146 available and CT remains the standard of care for NSCLC patients); 8) did not reach a
147 sufficient quality score according to the quality assessment (described below).

148 *Quality assessment*

149 The methodological quality of each study for its possible inclusion in the quantitative
150 assessment was evaluated by using the Checklist for Artificial Intelligence in Medical
151 Imaging (CLAIM)¹¹. Classification, image reconstruction, text analysis, and workflow
152 optimization are some of the applications of AI in medical imaging that are addressed
153 by CLAIM, which is modeled after the Standards for Reporting of Diagnostic Accuracy
154 Studies (STARD) guideline¹²⁻¹⁵. CLAIM checklist consists of 42 items divided into the
155 conventional sections included in peer-reviewed scientific articles: title or abstract (1
156 item), abstract (1 item), introduction (2 items), methods (28 items subdivided into study
157 design [2 items], data [7 items], ground truth [5 items], data partitions [3 items], model [3
158 items], training [3 items] and evaluation [5 items]), results (5 items subdivided into
159 data [2 items] and model performance [3 items]), discussion (2 items) and other
160 information (3 items). The CLAIM guideline offers a roadmap for writers and reviewers
161 with the intention of fostering clear, open, and verifiable scientific discourse on the use
162 of AI in medical imaging¹¹.

163 For our quality assessment, a score was calculated for each paper ([total score, 42 -
164 number of “not applicable” fields in each case]). A cut-off value of at least half of the
165 total score after removing the “not applicable” items was established for the inclusion in
166 the quantitative analysis. Therefore, this cut-off value varied for each study depending
167 on the number of items that were applicable from among the 42 total items included in
168 the CLAIM checklist (e.g., a cut-off value of 19 was established for those studies in
169 which only 38 items of the checklist were applicable). **See Supplementary Table S2.**
170 The assessment of the rigor, quality, and generalizability of the work of all enrolled
171 studies was performed by three reviewers (A.J.P., F.B.B. and A.P.P.).

172 **Data extraction**

173 Data extracted included the following: (1) study details: first author, publication year,
174 research questions, study design; (2) patient details: the source of data acquisition
175 (single-center/multicenter), sample size, smoking history, age, sex, TNM staging,
176 treatment status (naïve or any treatment received prior image acquisition), histological
177 subtype; (3) imaging details: imaging modality, plain or contrast CT; (4) oncogene
178 mutation status-related information: type of mutation, specific subtype of mutation (if
179 available), sequencing method; sequencing kit (5) radiomics details: segmentation
180 software, type of segmentation (manual, automatic, or semi-automatic), radiomics
181 feature extraction software, number of imaging features extracted, number and name of
182 radiomics features included in final models, features selection methods, type of models
183 constructed (machine learning [ML], deep learning [DL], classical statistical model),
184 final classifier used in machine learning models, clinical variables included in the
185 models (if applicable), and models performance. Two independent reviewers (A.F.M.
186 and A.L.S.) completed the initial screening and extracted data from all included studies.

187 **Data analysis**

188 For studies including models based on features extracted from different imaging
189 modalities, only those based on CT scans were included in the quantitative analysis. A
190 bivariate analysis of sensitivity and specificity as proposed by Reitsma et al.¹⁶ was
191 chosen to perform the meta-analyses. This method has the distinct advantage of
192 preserving the two-dimensional nature of the underlying data. It can also produce
193 summary estimates of sensitivity and specificity (false positive rate [FPR, 1-
194 specificity]), recognizing any possible correlation between these two measures. The

195 method uses a random effect approach in which the values of the sensitivity and FPR
196 estimates are obtained with restricted maximum likelihood. As a complement to the
197 bivariate approach, the summary receiver operating characteristic (sROC) was
198 calculated by converting each pair of sensitivity and specificity into a single measure of
199 accuracy, the diagnostic odds ratio (DOR).

200 The analyses were carried out by reproducing the confusion matrices of each model
201 presented in the studies, the number of cases and the prevalence of oncogene mutant
202 positive cases. All calculations were performed on the basis of validation cohorts for
203 studies applying a training/validation split method, or on the basis of the total sample
204 when cross-validation was the validation strategy. To ensure homogeneity, calculations
205 were conducted based on internal validation cohort data when external validation was
206 also performed (minority of the cases).

207 Finally, a meta-regression analysis was performed to measure the possible influence of
208 the following predictors: (1) average age of the cases, (2) manual segmentation vs semi-
209 automatic segmentation vs both procedures (no studies including automatic
210 segmentation approaches met the inclusion criteria for the quantitative analysis), (3)
211 whether the model included only radiomics features or was combined with clinical
212 variables, and (4) whether the model was classified as ML or DL. The heterogeneity in
213 the description of the clinical variables included in the models prevented the inclusion
214 of additional predictors of greatest clinical interest. Only the best model from each
215 study according to its DOR was selected. When the mean/median age was not available
216 due to the heterogeneity among studies when presenting descriptive results, it was
217 inferred from the information obtained. Thus, mean and median values were indistinctly
218 considered; when both values were provided, an average of both was calculated. If
219 mean values were absent, median values were considered and viceversa. If both values
220 were absent from the validation cohort, mean/median age from the total cohort was
221 considered. When this information was not available either, the study was not included
222 in the meta-regression.

223 All the analyses were performed using R Statistical Software v4.2.2 and the packages
224 mada and tidyverse.

225 **RESULTS**

226 In total 615 articles were obtained according to the search strategy (**Figure 1**). After de-
227 duplication, 397 studies were obtained and screened. According to the inclusion and
228 exclusion criteria, 89 studies were included in the qualitative analysis (systematic
229 review), all of them developing models for the prediction of EGFR, ALK, and/or
230 KRAS. Out of those, 38 were found eligible for the quantitative part of the study (meta-
231 analyses). As detailed in **Supplementary Table S2**, all papers passed this quality check
232 and were therefore included.

233 **Qualitative analysis (systematic review)**

234 *Methodological characteristics of the studies*

235 The methodological characteristics of the studies are summarized in **Table 1**. Most of
236 the studies ($n = 69/ 89$) applied exclusively ML algorithms, while this methodology was
237 also used to build comparator models in 10 articles in which DL techniques were the
238 main methodological approach followed. Only three studies exclusively applied DL
239 algorithms, while classical statistical models were used in seven publications. Among
240 the 79 articles applying ML techniques, the most common classifier used was logistic
241 regression ($n = 38$), followed by support vector machine ($n = 35$) and by random forest
242 ($n = 29$). In terms of partitioning strategy, training-validation split was the most frequent
243 technique ($n = 71$). External validation was only performed in a small set of studies
244 ($n = 9$). Regarding imaging techniques, CT was the most frequently used modality
245 ($n = 61$), followed by PET/CT ($n = 22$) and by PET alone ($n = 4$). Additionally, in one
246 study¹⁷ PET/CT scans and contrast-enhanced CT images independently acquired were
247 collected, while in another study¹⁸, PET/CT, CT, and contrast-enhanced diagnostic
248 quality (CTD) images were used. Of the 61 studies conducted with CT scans, 39
249 included non-contrast-enhanced images, 18 contrast-enhanced images, in two contrast-
250 related information was not specified and in two both contrast- and non-contrast-
251 enhanced scans were included. Regarding tumor segmentation, a manual approach was
252 followed in 48 studies, and automatic and semi-automatic segmentations were applied
253 in two and 31 studies, respectively; three studies applied both methodologies (for
254 verification or a different approach according to the imaging modality used) and five
255 studies did not specify the method utilized for tumor segmentation.

256 *Clinical characteristics of the studies*

257 The 89 studies evaluated in the qualitative synthesis included a total of 32,084 patients
258 with NSCLC. Although most of the studies included >200 patients, in 42 publications,
259 the sample size did not reach this figure and in 11 studies sample size was even lower
260 than 100. All studies were retrospective and mostly unicentric ($n = 72$); the number of
261 participant centers was not specified in one study¹⁹. In general, basic clinical and
262 demographic information collected included sex, age, smoking status, TNM stage,
263 histology, and treatment status at the moment of image acquisition, although this
264 information was not available in 13, 9, 22, 34, 22 and 24 studies out of the 89 assessed,
265 respectively. The clinical characteristics of the patients included in the 89 studies are
266 depicted in **Table 2**. The median [range]/ mean \pm standard deviation (SD) age of
267 patients was 61.78 [59–64.17] years and 61.71 ± 3.64 years, respectively. In terms of
268 sex, the total population was balanced, with 13,574 females and 14,066 males. The
269 smoking history was available for 23,200 patients, and many were non-smokers
270 ($n = 12,813$); while smoking history was unknown for 1,146 patients. Out of the 55
271 studies detailing information about the TNM stage, the majority of them ($n = 40$)
272 included information about the four stages (I-IV), either provided per group or grouped
273 in stages I-II and stages III-IV. Among the 15 studies that did not include patients of all
274 stages, two studies included only early stage patients (stages I and II)^{20, 21}, two included
275 patients stage II-IV^{22, 23}, six included only patients of stages III and IV²⁴⁻²⁹ (three of
276 them with a majority of stage IV patients^{24, 27, 29}), and five included patients of stages I-
277 III without including the most advanced stage^{19, 30-33}. A total of 65 studies included
278 patients with adenocarcinoma: 43 exclusively including this histology subtype and 22
279 including other NSCLC histology types as well. Finally, in most of the cases ($n = 65$),
280 images were acquired before patients received any treatment, with two studies also
281 including post-treatment images^{34, 35}. In 24 studies, no information on treatment was
282 detailed, although in some of them image acquisition before surgery^{31, 36-41}, before
283 polymerase chain reaction (PCR)⁴², or before pathological diagnosis⁴³ was detailed as
284 an inclusion criterion. In five studies^{19, 44-47}, authors specify that patients had not
285 received radiotherapy or chemotherapy, but no information on targeted therapy was
286 provided. Finally, only one study⁴⁸ out of the 89 included in the systematic review,
287 which did not meet the inclusion criteria to be considered for the meta-analysis,
288 included patients who had received treatment with tyrosine kinase inhibitors (TKIs).

289 **Quantitative analysis (meta-analysis)**

290 A total of 38 studies met the inclusion criteria for the quantitative assessment
291 ($n = 17,066$ patients). Three main different meta-analyses including radiomics-based
292 models were conducted: 1) a meta-analysis including studies focused on the detection of
293 EGFR ($n = 34$ studies)^{17, 25-28, 32, 33, 36, 38, 39, 46, 49-71}; 2) a meta-analysis including studies
294 focused on the detection of ALK ($n = 3$ studies)⁷²⁻⁷⁴; 3) a meta-analysis including
295 studies focused on the detection of KRAS ($n = 4$ studies)^{47, 50, 54, 62}. In three studies,
296 authors developed models for the detection of both EGFR and KRAS^{50, 54, 62}.
297 Furthermore, a separate meta-analysis was conducted for combined models (radiomics
298 features + clinical variables) for the prediction of EGFR (not enough studies for ALK or
299 KRAS mutations). Studies included in all the meta-analyses conducted are summarized
300 in **Supplementary Table S3**. Details on the radiomics features included in the EGFR,
301 ALK, and KRAS models are summarized in **Supplementary Table S4**,
302 **Supplementary Table S5** and **Supplementary Table S6**, respectively. In terms of
303 radiomics variables, models grouped different combinations of first order, shape, gray
304 level co-occurrence matrix (GLCM), gray level size zone matrix (GLSZM), gray level
305 run length matrix (GLRLM), neighboring gray tone difference matrix (NGTDM), and
306 gray level dependence matrix (GLDM) features. Clinical data included sex, smoking
307 history, and/or histological type in the majority of studies.

308 *EGFR*

309 Results of the meta-analysis focused on models built with radiomics features are
310 summarized in **Figure 2**. Note that this meta-analysis also included a study⁵⁰ in which
311 predictions were based on features extracted by a multi-channel and multi-task deep
312 learning model with the ability to simultaneously detect EGFR and KRAS oncogene
313 mutations; and consequently, did not include radiomics features (only single-task results
314 for the independent prediction of EGFR and KRAS were considered for the quantitative
315 analysis). A hierarchical sROC curve was plotted for the included 24 studies^{17, 25, 27, 32,}
316 ^{36, 39, 46, 49-51, 54, 55, 57-60, 62, 64-66, 68-71} that evaluate the performance of AI algorithms in
317 predicting EGFR mutation status in NSCLC (**Supplementary Figure S1**). Eight studies
318 assessed more than one model^{32, 36, 39, 50, 59, 60, 65, 70}. As observed, radiomics-based models
319 exhibited high diagnostic performance in predicting EGFR mutation status with an
320 overall AUC of 0.766. The AI algorithms' sensitivity in determining the EGFR mutation

321 status varied from 0.362 to 0.948, resulting in an estimate of 0.753 (95% CI 0.721–
322 0.783). The FPR of these algorithms ranged from 0.022 to 0.761, with a estimate of
323 0.346 (95% CI 0.305–0.390). Detecting a positive case for EGFR mutation was almost
324 six times more likely than not detecting it (DOR = 5.70 [95% CI 4.74–6.81]).

325 The effect of adding clinical variables to radiomics models or to models including both
326 radiomics and deep features⁶⁵ (models including clinical data and radiomic or deep
327 features referred in this work as combined models) in the prediction of EGFR mutation
328 was also analyzed. This meta-analysis included 23 studies^{25, 26, 28, 32, 33, 38, 39, 46, 51-53, 56-58,}
329 ⁶¹⁻⁶⁹, of which four of them developed more than one model^{32, 39, 56, 67}. Results are
330 depicted in **Figure 3** and sROC curve in **Supplementary Figure S1**. Overall, the
331 performance of combined models slightly improved compared to radiomics models,
332 with an AUC of 0.811 and a sensitivity of 0.800 (95% CI 0.767–0.830; model’s
333 sensitivity ranging from 0.523 to 0.944). The FPR resulted similar with a value of 0.335
334 (95% CI 0.279–0.396; model’s FPR ranging from 0.167 to 0.760.). Detecting a positive
335 case for EGFR mutation with combined models was more than eight times more likely
336 than not detecting it (DOR = 8.35 [95% CI 6.77–10.20]).

337 *ALK*

338 The meta-analysis focused on radiomics-based models included three studies⁷²⁻⁷⁴, one of
339 which developed two different models, one based on pre-contrast images and another
340 one on post-contrast images⁷³. An overall AUC of 0.831 was obtained for the prediction
341 of ALK aberration, with a sensitivity ranging from 0.682 to 0.825, resulting in an
342 estimate of 0.754 (95% CI 0.639–0.841). The FPR of these algorithms ranged from
343 0.167 to 0.277, with an estimate of 0.225 (95% CI 0.163–0.302). Detecting a positive
344 case for ALK aberration was 11 times more likely than not detecting it (DOR = 5.70
345 [95% CI 5.83–19.10]) (**Figure 4** and **Supplementary Figure S2**). Given the lack of
346 enough studies developing combined models, a meta-analysis to assess the effects of
347 adding clinical variables in the prediction of ALK aberration was not possible. The only
348 study⁷⁴ that developed a model including age, sex, smoking history, smoking index,
349 clinical stage, distal metastasis and pathological invasiveness of the tumor in
350 combination with conventional CT features and different first order, GLCM, GLSZM,
351 and GLRL radiomics features demonstrated increased performance in predicting ALK
352 aberration of the combined model vs the radiomics-based model, but only in the

353 primary cohort (AUC , 0.83–0.88, $p = 0.01$), not in the testing cohort (AUC , 0.80–0.88,
354 $p = 0.29$).

355 *KRAS*

356 Four studies met the inclusion criteria for the meta-analysis assessing models for *KRAS*
357 mutation prediction^{47, 50, 54, 62}, among which, three of them also developed models for
358 *EGFR* mutation prediction^{50, 54, 62}. *KRAS/EGFR* models were independently built
359 except in one study, in which a multi-channel multi-task DL model for the prediction of
360 both *KRAS* and *EGFR* mutations was developed⁵⁰. However, and according to the
361 inclusion criteria, only single-task metrics were considered for the quantitative analysis
362 despite the multi-channel version displayed the highest performance for the
363 simultaneous detection of both oncogenic driver mutations. Results of the meta-analysis
364 evaluating radiomics-based models are shown in **Figure 4** and **Supplementary Figure**
365 **S3**. *KRAS* mutation was predicted with an overall AUC of 0.732 and a sensitivity of
366 0.744 (95% CI 0.605–0.846; model’s sensitivity ranging from 0.641 to 0.875. The FPR
367 was 0.376 (95% CI 0.274–0.491; model’s FPR ranging from 0.259 to 0.468). Detecting
368 a positive case for *KRAS* mutation with radiomics-based models was more than five
369 times more likely than not detecting it (DOR = 8.35 [95% CI 1.98–11.70]). Like *ALK*,
370 the lack of enough *KRAS* studies made it impossible to perform a meta-analysis
371 analyzing combined models. Only Ríos Velázquez et al.⁶² built a model including age,
372 sex, smoking status, race, and clinical stage together with radiomics features that
373 performed similar to the radiomics model (AUC = 0.69 [95% CI: 0.63– 0.75] vs
374 AUC = 0.63 [95% CI: 0.57– 0.69]) and worse than a model developed only with clinical
375 data AUC = 0.75 [95% CI: 0.69–0.80].

376 *Meta-regression and subgroup analysis*

377 The possible effects of different predictors on the predictive performance of the models
378 was evaluated for *EGFR* mutation (not enough studies were available for *ALK* or
379 *KRAS* mutations). Neither age, nor the use of contrast, nor the type of segmentation
380 (manual/semi-automatic/automatic), nor the model (radiomics/combined), nor the AI
381 methodology (machine learning/deep learning), yielded statistically significant results
382 (**Supplementary Table S7**).

383 **DISCUSSION**

384 At present, molecular testing performed on biopsied tissue remains the gold standard for
385 diagnosis and genotyping in advanced NSCLC^{75, 76}. However, given the associated
386 limitations and inconveniences, such as the lack of enough tissue for successful
387 testing^{77, 78}, or the long turnaround times⁷⁶, there is a need to validate and incorporate
388 new procedures into routine clinical practice. In recent years, liquid biopsy has emerged
389 as a promising alternative in NSCLC, especially in clinical scenarios⁷⁸. Likewise,
390 radiomics have shown encouraging results in prognosis and prediction in this setting⁷⁹.
391 In general, both methodologies possess great potential, since they are both simple,
392 straightforward to do, and repeatable at patient follow-up visits, which makes it possible
393 to gather important data about the type of tumor, its aggressiveness, its progression, and
394 its response to therapy⁸⁰. Radiomics has the additional advantage of only requiring
395 medical images and capturing patient-level and tissue-level heterogeneity, such as CT
396 scans in lung cancer, that are usually acquired as part of the patient's standard journey,
397 representing an affordable methodology both in terms of resources and costs. It is
398 important that new techniques are properly validated to facilitate their standardization,
399 prior to incorporation into the routine clinical workflow.

400 To our knowledge, this is the first systematic review and meta-analysis that analyzes the
401 performance and applicability of different imaging-based models for the prediction of
402 three of the most common oncogene mutations—EGFR, ALK and KRAS—in NSCLC
403 from a clinical perspective and with a special focus on AI methodologies. So far, results
404 were only available for EGFR studies and did not take clinical aspects into account⁸¹.
405 Thus, the results of our different meta-analyses demonstrate that AI-based models
406 developed with CT-derived radiomics features showed good performance in predicting
407 EGFR, ALK, and KRAS mutations with a sensitivity of 0.753 [95% CI (0.721–0.783)],
408 0.754 [95% CI (0.639–0.841)] and 0.744 [95% CI (0.605–0.846)], respectively.
409 Whether the inclusion of clinical variables increase models' performance cannot be
410 concluded from our results, although we believe that increasing the number of studies
411 would probably confirm the trends observed in our quantitative analysis of EGFR
412 mutation.

413 Our outcomes point to radiomics as a candidate screening tool for oncogene mutation
414 status determination. We especially focused on CT-based models, aiming to obtain

415 conclusions as applicable as possible to the standard clinical workflow since CT
416 remains the most utilized imaging tool in NSCLC⁸². From our work, we conclude that
417 in addition to additional validation of our findings that future studies should be
418 conducted that consider the following important aspects. Firstly, a minimum sample size
419 should be guaranteed to ensure the reliability of the results obtained with AI-based
420 models^{83, 84}. In both our systematic review and meta-analyses, more than half of the
421 studies were conducted in >200 patients ($n = 46/89$ and $n = 23/38$ [$n = 20/34$ for EGFR,
422 $n = 2/3$ for ALK and $n = 3/4$ for KRAS]), but still a sizable number had small sample
423 sizes, which definitely limited the relevance of their conclusions. Multicentric designs
424 would be also desirable to get more solid conclusions, an approach that few studies
425 followed ($n = 16/89$ in the systematic review and $n = 10/39$ in the meta-analysis
426 [$n = 10/34$ for EGFR, $n = 0/3$ for ALK and $n = 3/4$ for KRAS]). Secondly, including
427 independent cohorts for external validations would reinforce the results, leading to more
428 robust and reproducible models. Out of the 89 studies included in the qualitative
429 analysis, only 9 used external cohorts for validation^{43, 46, 60, 63, 67, 68, 85-87}, of which five
430 were included in the EGFR meta-analysis^{46, 60, 63, 67, 68}. Finally, it is important that
431 patient populations reflect clinical practice. Thus, considering the potential applicability
432 of the models for diagnostic purposes, studies should be conducted in treatment naïve
433 populations to avoid possible therapy-related confounding effects, an inclusion criterion
434 mostly applied in the studies evaluated in this work, but still missing in some of them.
435 Additionally, studies should be carried out preferably in stage III-IV NSCLC patients
436 (especially in those at stage IV, for whom clinical guidelines recommend molecular
437 testing^{75, 76}). As demonstrated in this work, most of the studies published so far do not
438 provide information on TNM stage or include patients from all stages. Despite the
439 heterogeneity of the studies evaluated, we believe that the evidence provided is enough
440 as to demonstrate the potential of radiomics in oncogene mutation status determination.
441 Thus, AI-based models using radiomics extracted from CT scans could be effective non-
442 invasive screening tools to detect targetable driver mutations in NSCLC with good
443 sensitivity and moderate specificity. These tools would not be intended to replace gold
444 standard techniques, such as PCR or next-generation sequencing, but to allow for the
445 potential earlier identification of ideal candidates to be genetically tested, saving time,
446 costs, and samples. Consequently, a high sensitivity would ensure the identification of
447 oncogene mutation positive patients for whom laboratory-based testing would be
448 subsequently confirmed.

449 When the influence of different factors on the prediction of EGFR mutation was
450 evaluated, no statistically significant results were obtained, probably due to the limited
451 number of studies included and the presence of missing data. However, some of those
452 factors might play an essential role and should be considered when developing accurate
453 models to be potentially implemented into clinical practice. Indeed, some of the studies
454 included in our qualitative analysis analyzed the impact of different methodological
455 aspects on the performance of the models. For example, Huang et al.³⁵ demonstrated
456 that interobserver variability in tumor segmentation affects the use of radiomics to
457 predict oncogene mutation status, which suggests that automatic or semi-automatic
458 models might be more suitable. In the study by Shiri et al.⁸⁸, the application to
459 radiomics features of ComBat harmonization improved the performance of the models
460 toward more successful prediction of EGFR and KRAS mutations. Likewise, other
461 authors have pointed to the impact of the experimental settings on the robustness of
462 radiomics features⁸⁹, or the influence of CT slice thickness on the predictive
463 performance of radiomics-based models³¹. It is also worth mentioning the relevance of
464 using a particular AI methodology. Although we found no differences in the EGFR
465 mutation predictive performance between ML and DL methods, most likely due to the
466 limited number of available DL-based studies, the latter might offer some advantages
467 over the former. Thus, while in radiomics analysis a process of lesion segmentation and
468 subsequent feature extraction is required, which introduces certain degree of variability
469 and can be a high time-consuming task, DL models only required a bounding box of the
470 lesion, greatly reducing this effect. On the other hand, DL models, and in particular end-
471 to-end convolutional neural network (CNN) models, such those developed in most of
472 the DL studies included in our work^{37, 42, 43, 50, 58, 68, 85, 86, 90, 91}, are generally more
473 complex in terms of the number of parameters, allowing to solve more complicated
474 problems than traditional ML models. Considering available evidence, it seems
475 reasonable to think that methodologic approaches should be carefully revised when
476 validation studies are designed and conducted.

477 Our study has also some limitations, mainly derived from the limitations of the
478 publications included. Thus, it is based on retrospective studies displaying great
479 heterogeneity in terms of methodology and patient clinical characteristics, which clearly
480 hamper the impact of our conclusions. Additionally, the limited available evidence for
481 ALK and KRAS mutations, makes it difficult to draw solid conclusions. Despite this,

482 our work gathers the most up-to-date and complete evidence (all models developed in
483 each of the studies were analyzed) on imaging-based models for the prediction of three
484 of the most important oncogene mutations in NSCLC, following a clinical approach and
485 a special focus on AI models. Our exhaustive review and meta-analyses are intended to
486 provide solid evidence for future research in the field.

487 In conclusion, radiomics-based models offer a useful and non-invasive method for
488 determining the status of EGFR mutations in NSCLC and seem to retain similar
489 predictive value for ALK and KRAS mutations. Additionally, although the inclusion of
490 clinical variables tends to increase the performance of the models, further validation is
491 required.

492 **ACKNOWLEDGEMENTS**

493

494 **CONFLICTS OF INTEREST**

495 GJW reports personal fees from Quibim related to this work. He is a former employee
496 of SOTIO Biotech Inc., and reports personal fees from Imaging Endpoints II,
497 MiRanostics Consulting, Gossamer Bio, International Genomics Consortium, Angiex,
498 Genomic Health, Oncacare, Rafael Pharmaceuticals, Roche, Immunocore, Kymera, and
499 SPARC-all outside this submitted work; has ownership interest in MiRanostics
500 Consulting, Exact Sciences, Moderna, Agenus, Aurinia Pharmaceuticals, and
501 Circulogene-outside the submitted work; and has issued patents- all outside the
502 submitted work. The remaining authors declare no conflicts of interest.

503 **FUNDING**

504

505 **REFERENCES**

- 506 1 Sung H, Ferlay J, Siegel RL et al. Global Cancer Statistics 2020: GLOBOCAN
507 estimates of incidence and mortality worldwide for 36 Cancers in 185 countries.
508 *CA Cancer J Clin.* 2021; 71(3): 209-249.
- 509 2 Osmani L, Askin F, Gabrielson E et al. Current WHO guidelines and the critical
510 role of immunohistochemical markers in the subclassification of non-small cell
511 lung carcinoma (NSCLC): moving from targeted therapy to immunotherapy.
512 *Semin Cancer Biol.* 2018; 52(Pt 1): 103-109.

- 513 3 König D, Savic Prince S, Rothschild SI. Targeted therapy in advanced and
514 metastatic non-small cell lung cancer. An update on treatment of the most
515 important actionable oncogenic driver alterations. *Cancers (Basel)*. 2021; 13(4).
- 516 4 Chiu YW, Kao YH, Simoff MJ et al. Costs of biopsy and complications in
517 patients with lung cancer. *Clinicoecon Outcomes Res*. 2021; 13: 191-200.
- 518 5 Manicone M, Poggiana C, Facchinetti A et al. Critical issues in the clinical
519 application of liquid biopsy in non-small cell lung cancer. *J Thorac Dis*. 2017;
520 9(Suppl 13): S1346-s1358.
- 521 6 Young M SR. Percutaneous lung lesion biopsy. [Updated 2023 Jun 19].
522 *StatPearls [Internet]*. . Treasure Island (FL): StatPearls Publishing.
- 523 7 Di Capua D, Bracken-Clarke D, Ronan K et al. The liquid biopsy for lung
524 cancer: state of the art, limitations and future developments. *Cancers (Basel)*.
525 2021; 13(16).
- 526 8 Wu G, Jochems A, Refaee T et al. Structural and functional radiomics for lung
527 cancer. *Eur J Nucl Med Mol Imaging*. 2021; 48(12): 3961-3974.
- 528 9 Bera K, Braman N, Gupta A et al. Predicting cancer outcomes with radiomics
529 and artificial intelligence in radiology. *Nat Rev Clin Oncol*. 2022; 19(2): 132-
530 146.
- 531 10 Page MJ, McKenzie JE, Bossuyt PM et al. The PRISMA 2020 statement: an
532 updated guideline for reporting systematic reviews. *BMJ*. 2021; 372: n71.
- 533 11 Mongan J, Moy L, Kahn CE. Checklist for artificial intelligence in medical
534 imaging (CLAIM): a guide for authors and reviewers. *Radiol Artif Intell*. 2020;
535 2(2): e200029.
- 536 12 Bossuyt PM, Reitsma JB. The STARD initiative. *Lancet*. 2003; 361(9351): 71.
- 537 13 Bossuyt PM, Reitsma JB, Bruns DE et al. Towards complete and accurate
538 reporting of studies of diagnostic accuracy: the STARD initiative. *Radiology*.
539 2003; 226(1): 24-28.
- 540 14 Bossuyt PM, Reitsma JB, Bruns DE et al. STARD 2015: an updated list of
541 essential items for reporting diagnostic accuracy studies. *Radiology*. 2015;
542 277(3): 826-832.
- 543 15 Cohen JF, Korevaar DA, Altman DG et al. STARD 2015 guidelines for reporting
544 diagnostic accuracy studies: explanation and elaboration. *BMJ Open*. 2016;
545 6(11): e012799.
- 546 16 Reitsma JB, Glas AS, Rutjes AW et al. Bivariate analysis of sensitivity and
547 specificity produces informative summary measures in diagnostic reviews. *J*
548 *Clin Epidemiol*. 2005; 58(10): 982-990.
- 549 17 Nair JKR, Saeed UA, McDougall CC et al. Radiogenomic models using
550 machine learning techniques to predict EGFR mutations in non-small cell lung
551 cancer. *Can Assoc Radiol J*. 2021; 72(1): 109-119.
- 552 18 Shiri I, Maleki H, Hajianfar G et al. Next-generation radiogenomics sequencing
553 for prediction of EGFR and KRAS mutation status in NSCLC patients using

- 554 multimodal imaging and machine learning algorithms. *Mol Imaging Biol.* 2020;
555 22(4): 1132-1148.
- 556 19 Dang Y, Wang R, Qian K et al. Clinical and radiological predictors of epidermal
557 growth factor receptor mutation in nonsmall cell lung cancer. *J Appl Clin Med*
558 *Phys.* 2021; 22(1): 271-280.
- 559 20 Omura K, Murakami Y, Hashimoto K et al. Detection of EGFR mutations in
560 early-stage lung adenocarcinoma by machine learning-based radiomics. *Transl*
561 *Cancer Res.* 2023; 12(4): 837-847.
- 562 21 Wang X, Kong C, Xu W et al. Decoding tumor mutation burden and driver
563 mutations in early stage lung adenocarcinoma using CT-based radiomics
564 signature. *Thorac Cancer.* 2019; 10(10): 1904-1912.
- 565 22 Liu Q, Sun D, Li N et al. Predicting EGFR mutation subtypes in lung
566 adenocarcinoma using (18)F-FDG PET/CT radiomic features. *Transl Lung*
567 *Cancer Res.* 2020; 9(3): 549-562.
- 568 23 Yang L, Xu P, Li M et al. PET/CT radiomic features: a potential biomarker for
569 EGFR mutation status and survival outcome prediction in NSCLC patients
570 treated with TKIs. *Front Oncol.* 2022; 12: 894323.
- 571 24 Hong D, Xu K, Zhang L et al. Radiomics signature as a predictive factor for
572 EGFR mutations in advanced lung adenocarcinoma. *Front Oncol.* 2020; 10: 28.
- 573 25 Lu J, Ji X, Wang L et al. Machine learning-based radiomics for prediction of
574 epidermal growth factor receptor mutations in lung adenocarcinoma. *Dis*
575 *Markers.* 2022; 2022: 2056837.
- 576 26 Wu S, Shen G, Mao J et al. CT radiomics in predicting EGFR mutation in non-
577 small cell lung cancer: a single institutional study. *Front Oncol.* 2020; 10:
578 542957.
- 579 27 Yang C, Chen W, Gong G et al. Application of CT radiomics features to predict
580 the EGFR mutation status and therapeutic sensitivity to TKIs of advanced lung
581 adenocarcinoma. *Transl Cancer Res.* 2020; 9(11): 6683-6690.
- 582 28 Zhang L, Chen B, Liu X et al. Quantitative biomarkers for prediction of
583 epidermal growth factor receptor mutation in non-small cell lung cancer. *Transl*
584 *Oncol.* 2018; 11(1): 94-101.
- 585 29 Zhu Y, Guo YB, Xu D et al. A computed tomography (CT)-derived radiomics
586 approach for predicting primary co-mutations involving TP53 and epidermal
587 growth factor receptor (EGFR) in patients with advanced lung adenocarcinomas
588 (LUAD). *Ann Transl Med.* 2021; 9(7): 545.
- 589 30 Aide N, Weyts K, Lasnon C. Prediction of the presence of targetable molecular
590 alteration(s) with clinico-metabolic (18) F-FDG PET radiomics in non-Asian
591 lung adenocarcinoma patients. *Diagnostics (Basel).* 2022; 12(10).
- 592 31 Li Y, Lu L, Xiao M et al. CT slice thickness and convolution Kernel affect
593 performance of a radiomic model for predicting egfr status in non-small cell
594 lung cancer: a preliminary study. *Sci Rep.* 2018; 8(1): 17913.

- 595 32 Zhu H, Song Y, Huang Z et al. Accurate prediction of epidermal growth factor
596 receptor mutation status in early-stage lung adenocarcinoma, using radiomics
597 and clinical features. *Asia Pac J Clin Oncol*. 2022; 18(6): 586-594.
- 598 33 Dong Y, Jiang Z, Li C et al. Development and validation of novel radiomics-
599 based nomograms for the prediction of EGFR mutations and Ki-67 proliferation
600 index in non-small cell lung cancer. *Quant Imaging Med Surg*. 2022; 12(5):
601 2658-2671.
- 602 34 Aerts HJ, Grossmann P, Tan Y et al. Defining a radiomic response phenotype: a
603 pilot study using targeted therapy in NSCLC. *Sci Rep*. 2016; 6: 33860.
- 604 35 Huang Q, Lu L, Dercle L et al. Interobserver variability in tumor contouring
605 affects the use of radiomics to predict mutational status. *J Med Imaging*
606 *(Bellingham)*. 2018; 5(1): 011005.
- 607 36 Feng Y, Song F, Zhang P et al. Prediction of EGFR mutation status in non-small
608 cell lung cancer based on ensemble learning. *Front Pharmacol*. 2022; 13:
609 897597.
- 610 37 Huang X, Sun Y, Tan M et al. Three-dimensional convolutional neural network-
611 based prediction of epidermal growth factor receptor expression status in
612 patients with non-small cell lung cancer. *Front Oncol*. 2022; 12: 772770.
- 613 38 Jia TY, Xiong JF, Li XY et al. Identifying EGFR mutations in lung
614 adenocarcinoma by noninvasive imaging using radiomics features and random
615 forest modeling. *Eur Radiol*. 2019; 29(9): 4742-4750.
- 616 39 Liu G, Xu Z, Ge Y et al. 3D radiomics predicts EGFR mutation, exon-19
617 deletion and exon-21 L858R mutation in lung adenocarcinoma. *Transl Lung*
618 *Cancer Res*. 2020; 9(4): 1212-1224.
- 619 40 Mei D, Luo Y, Wang Y et al. CT texture analysis of lung adenocarcinoma: can
620 Radiomic features be surrogate biomarkers for EGFR mutation statuses. *Cancer*
621 *Imaging*. 2018; 18(1): 52.
- 622 41 Zhang T, Xu Z, Liu G et al. Simultaneous identification of
623 EGFR, KRAS, ERBB2, and TP53 mutations in patients with non-small cell lung
624 cancer by machine learning-derived three-dimensional radiomics. *Cancers*
625 *(Basel)*. 2021; 13(8).
- 626 42 Song J, Ding C, Huang Q et al. Deep learning predicts epidermal growth factor
627 receptor mutation subtypes in lung adenocarcinoma. *Med Phys*. 2021; 48(12):
628 7891-7899.
- 629 43 Wang C, Xu X, Shao J et al. Deep learning to predict EGFR mutation and PD-
630 L1 expression status in non-small-cell lung cancer on computed tomography
631 images. *J Oncol*. 2021; 2021: 5499385.
- 632 44 Huang W, Wang J, Wang H et al. PET/CT based egfr mutation status
633 classification of NSCLC using deep learning features and radiomics features.
634 *Front Pharmacol*. 2022; 13: 898529.
- 635 45 Kawazoe Y, Shiinoki T, Fujimoto K et al. Investigation of the combination of
636 intratumoral and peritumoral radiomic signatures for predicting epidermal

- 637 growth factor receptor mutation in lung adenocarcinoma. *J Appl Clin Med Phys*.
638 2023; 24(6): e13980.
- 639 46 Lu X, Li M, Zhang H et al. A novel radiomic nomogram for predicting
640 epidermal growth factor receptor mutation in peripheral lung adenocarcinoma.
641 *Phys Med Biol*. 2020; 65(5): 055012.
- 642 47 Wang J, Lv X, Huang W et al. Establishment and optimization of radiomics
643 algorithms for prediction of KRAS gene mutation by integration of NSCLC
644 gene mutation mutual exclusion information. *Front Pharmacol*. 2022; 13:
645 862581.
- 646 48 Yang X, Fang C, Li C et al. Can CT radiomics detect acquired T790M mutation
647 and predict prognosis in advanced lung adenocarcinoma with progression after
648 first- or second-generation EGFR TKIs? *Front Oncol*. 2022; 12: 904983.
- 649 49 Chang C, Zhou S, Yu H et al. A clinically practical radiomics-clinical combined
650 model based on PET/CT data and nomogram predicts EGFR mutation in lung
651 adenocarcinoma. *Eur Radiol*. 2021; 31(8): 6259-6268.
- 652 50 Dong Y, Hou L, Yang W et al. Multi-channel multi-task deep learning for
653 predicting EGFR and KRAS mutations of non-small cell lung cancer on CT
654 images. *Quant Imaging Med Surg*. 2021; 11(6): 2354-2375.
- 655 51 Gao J, Niu R, Shi Y et al. The predictive value of [(18)F]FDG PET/CT
656 radiomics combined with clinical features for EGFR mutation status in different
657 clinical staging of lung adenocarcinoma. *EJNMMI Res*. 2023; 13(1): 26.
- 658 52 Huo JW, Luo TY, Diao L et al. Using combined CT-clinical radiomics models to
659 identify epidermal growth factor receptor mutation subtypes in lung
660 adenocarcinoma. *Front Oncol*. 2022; 12: 846589.
- 661 53 Jiang M, Yang P, Li J et al. Computed tomography-based radiomics
662 quantification predicts epidermal growth factor receptor mutation status and
663 efficacy of first-line targeted therapy in lung adenocarcinoma. *Front Oncol*.
664 2022; 12: 985284.
- 665 54 Le NQK, Kha QH, Nguyen VH et al. Machine learning-based radiomics
666 signatures for EGFR and KRAS mutations prediction in non-small-cell lung
667 cancer. *Int J Mol Sci*. 2021; 22(17).
- 668 55 Li S, Li Y, Zhao M et al. Combination of (18)F-fluorodeoxyglucose PET/CT
669 radiomics and clinical features for predicting epidermal growth factor receptor
670 mutations in lung adenocarcinoma. *Korean J Radiol*. 2022; 23(9): 921-930.
- 671 56 Li S, Luo T, Ding C et al. Detailed identification of epidermal growth factor
672 receptor mutations in lung adenocarcinoma: Combining radiomics with machine
673 learning. *Med Phys*. 2020; 47(8): 3458-3466.
- 674 57 Li X, Yin G, Zhang Y et al. Predictive power of a radiomic signature based on
675 (18)F-FDG PET/CT images for EGFR mutational status in NSCLC. *Front
676 Oncol*. 2019; 9: 1062.
- 677 58 Li XY, Xiong JF, Jia TY et al. Detection of epithelial growth factor receptor
678 (EGFR) mutations on CT images of patients with lung adenocarcinoma using

- 679 radiomics and/or multi-level residual convolutionary neural networks. *J Thorac*
680 *Dis.* 2018; 10(12): 6624-6635.
- 681 59 Liu Y, Zhou J, Wu J et al. Development and validation of machine learning
682 models to predict epidermal growth factor receptor mutation in non-small cell
683 lung cancer: a multi-center retrospective radiomics study. *Cancer Control.* 2022;
684 29: 10732748221092926.
- 685 60 Ninomiya K, Arimura H, Chan WY et al. Robust radiogenomics approach to the
686 identification of EGFR mutations among patients with NSCLC from three
687 different countries using topologically invariant Betti numbers. *PLoS One.* 2021;
688 16(1): e0244354.
- 689 61 Ninomiya K, Arimura H, Tanaka K et al. Three-dimensional topological
690 radiogenomics of epidermal growth factor receptor Del19 and L858R mutation
691 subtypes on computed tomography images of lung cancer patients. *Comput*
692 *Methods Programs Biomed.* 2023; 236: 107544.
- 693 62 Rios Velazquez E, Parmar C, Liu Y et al. Somatic mutations drive distinct
694 imaging phenotypes in lung cancer. *Cancer Res.* 2017; 77(14): 3922-3930.
- 695 63 Rossi G, Barabino E, Fedeli A et al. Radiomic detection of EGFR mutations in
696 NSCLC. *Cancer Res.* 2021; 81(3): 724-731.
- 697 64 Tu W, Sun G, Fan L et al. Radiomics signature: A potential and incremental
698 predictor for EGFR mutation status in NSCLC patients, comparison with CT
699 morphology. *Lung Cancer.* 2019; 132: 28-35.
- 700 65 Wang C, Ma J, Shao J et al. Predicting EGFR and PD-L1 status in NSCLC
701 patients using multitask ai system based on CT images. *Front Immunol.* 2022;
702 13: 813072.
- 703 66 Weng Q, Hui J, Wang H et al. Radiomic feature-based nomogram: a novel
704 technique to predict EGFR-activating mutations for EGFR tyrosin kinase
705 inhibitor therapy. *Front Oncol.* 2021; 11: 590937.
- 706 67 Yang X, Liu M, Ren Y et al. Using contrast-enhanced CT and non-contrast-
707 enhanced CT to predict EGFR mutation status in NSCLC patients-a radiomics
708 nomogram analysis. *Eur Radiol.* 2022; 32(4): 2693-2703.
- 709 68 Zhang B, Qi S, Pan X et al. Deep CNN model using CT radiomics feature
710 mapping recognizes EGFR gene mutation status of lung adenocarcinoma. *Front*
711 *Oncol.* 2020; 10: 598721.
- 712 69 Zhang G, Cao Y, Zhang J et al. Predicting EGFR mutation status in lung
713 adenocarcinoma: development and validation of a computed tomography-based
714 radiomics signature. *Am J Cancer Res.* 2021; 11(2): 546-560.
- 715 70 Zhang M, Bao Y, Rui W et al. Performance of (18)F-FDG PET/CT radiomics for
716 predicting EGFR mutation status in patients with non-small cell lung cancer.
717 *Front Oncol.* 2020; 10: 568857.
- 718 71 Zhao HY, Su YX, Zhang LH et al. Prediction model based on 18F-FDG PET/CT
719 radiomic features and clinical factors of EGFR mutations in lung
720 adenocarcinoma. *Neoplasma.* 2022; 69(1): 233-241.

- 721 72 Chang C, Sun X, Wang G et al. A machine learning model based on PET/CT
722 radiomics and clinical characteristics predicts ALK rearrangement status in lung
723 adenocarcinoma. *Front Oncol.* 2021; 11: 603882.
- 724 73 Ma DN, Gao XY, Dan YB et al. Evaluating solid lung adenocarcinoma
725 anaplastic lymphoma kinase gene rearrangement using noninvasive radiomics
726 biomarkers. *Onco Targets Ther.* 2020; 13: 6927-6935.
- 727 74 Song L, Zhu Z, Mao L et al. Clinical, conventional ct and radiomic feature-based
728 machine learning models for predicting ALK rearrangement status in lung
729 adenocarcinoma patients. *Front Oncol.* 2020; 10: 369.
- 730 75 Hendriks LE, Kerr KM, Menis J et al. Oncogene-addicted metastatic non-small-
731 cell lung cancer: ESMO clinical practice guideline for diagnosis, treatment and
732 follow-up. *Ann Oncol.* 2023; 34(4): 339-357.
- 733 76 Ettinger DS, Wood DE, Aisner DL et al. Non-Small Cell Lung Cancer, Version
734 3.2022, NCCN Clinical Practice Guidelines in Oncology. *J Natl Compr Canc*
735 *Netw.* 2022; 20(5): 497-530.
- 736 77 Ferry-Galow KV, Datta V, Makhlof HR et al. What can be done to improve
737 research biopsy quality in oncology clinical trials? *J Oncol Pract.* 2018; 14(11):
738 Jop1800092.
- 739 78 Gutierrez ME, Choi K, Lanman RB et al. Genomic profiling of advanced non-
740 small cell lung cancer in community settings: gaps and opportunities. *Clin Lung*
741 *Cancer.* 2017; 18(6): 651-659.
- 742 79 Fornacon-Wood I, Faivre-Finn C, O'Connor JPB et al. Radiomics as a
743 personalized medicine tool in lung cancer: separating the hope from the hype.
744 *Lung Cancer.* 2020; 146: 197-208.
- 745 80 Neri E, Del Re M, Paiar F et al. Radiomics and liquid biopsy in oncology: the
746 holons of systems medicine.
747 *Insights Imaging.* 2018; 9(6): 915-924.
- 748 81 Nguyen HS, Ho DKN, Nguyen NN et al. Predicting EGFR mutation status in
749 non-small cell lung cancer using artificial intelligence: a systematic review and
750 meta-analysis. *Acad Radiol.* 2023.
- 751 82 Steinert HC. PET and PET-CT of lung cancer. *Methods Mol Biol.* 2011; 727: 33-
752 51.
- 753 83 Alwosheel A, van Cranenburgh S, Chorus CG. Is your dataset big enough?
754 Sample size requirements when using artificial neural networks for discrete
755 choice analysis. *J Choice Model.* 2018; 28: 167-182.
- 756 84 Rajput D, Wang W-J, Chen C-C. Evaluation of a decided sample size in machine
757 learning applications. *BMC Bioinformatics.* 2023; 24(1): 48.
- 758 85 Mu W, Jiang L, Zhang J et al. Non-invasive decision support for NSCLC
759 treatment using PET/CT radiomics. *Nat Commun.* 2020; 11(1): 5228.
- 760 86 Zhao W, Yang J, Ni B et al. Toward automatic prediction of EGFR mutation
761 status in pulmonary adenocarcinoma with 3D deep learning. *Cancer Med.* 2019;
762 8(7): 3532-3543.

- 763 87 Zuo Y, Liu Q, Li N et al. Optimal (18)F-FDG PET/CT radiomics model
764 development for predicting EGFR mutation status and prognosis in lung
765 adenocarcinoma: a multicentric study. *Front Oncol.* 2023; 13: 1173355.
- 766 88 Shiri I, Amini M, Nazari M et al. Impact of feature harmonization on
767 radiogenomics analysis: prediction of EGFR and KRAS mutations from non-
768 small cell lung cancer PET/CT images. *Comput Biol Med.* 2022; 142: 105230.
- 769 89 Yip SSF, Parmar C, Kim J et al. Impact of experimental design on PET
770 radiomics in predicting somatic mutation status. *Eur J Radiol.* 2017; 97: 8-15.
- 771 90 Shao J, Ma J, Zhang S et al. Radiogenomic system for non-invasive
772 identification of multiple actionable mutations and PD-L1 expression in non-
773 small cell lung cancer based on ct images. *Cancers (Basel).* 2022; 14(19).
- 774 91 Xiao Z, Cai H, Wang Y et al. Deep learning for predicting epidermal growth
775 factor receptor mutations of non-small cell lung cancer on PET/CT images.
776 *Quant Imaging Med Surg.* 2023; 13(3): 1286-1299.
- 777 92 Ağuloğlu N, Aksu A, Akyol M et al. Importance of pretreatment 18F-FDG
778 PET/CT texture analysis in predicting EGFR and ALK mutation in patients with
779 non-small cell lung cancer. *Nuklearmedizin.* 2022; 61(6): 433-439.
- 780 93 Agazzi GM, Ravanelli M, Roca E et al. CT texture analysis for prediction of
781 EGFR mutational status and ALK rearrangement in patients with non-small cell
782 lung cancer. *Radiol Med.* 2021; 126(6): 786-794.
- 783 94 Chen W, Hua Y, Mao D et al. A computed tomography-derived radiomics
784 approach for predicting uncommon EGFR mutation in patients with NSCLC.
785 *Front Oncol.* 2021; 11: 722106.
- 786 95 Chen Q, Li Y, Cheng Q et al. EGFR mutation status and subtypes predicted by
787 CT-based 3D radiomic features in lung adenocarcinoma. *Onco Targets Ther.*
788 2022; 15: 597-608.
- 789 96 Choe J, Lee SM, Kim W et al. CT radiomics-based prediction of anaplastic
790 lymphoma kinase and epidermal growth factor receptor mutations in lung
791 adenocarcinoma. *Eur J Radiol.* 2021; 139: 109710.
- 792 97 Digumarthy SR, Padole AM, Gullo RL et al. Can CT radiomic analysis in
793 NSCLC predict histology and EGFR mutation status? *Medicine (Baltimore).*
794 2019; 98(1): e13963.
- 795 98 Hao P, Deng BY, Huang CT et al. Predicting anaplastic lymphoma kinase
796 rearrangement status in patients with non-small cell lung cancer using a machine
797 learning algorithm that combines clinical features and CT images. *Front Oncol.*
798 2022; 12: 994285.
- 799 99 He R, Yang X, Li T et al. A machine learning-based predictive model of
800 epidermal growth factor mutations in lung adenocarcinomas. *Cancers (Basel).*
801 2022; 14(19).
- 802 100 Hou D, Li W, Wang S et al. Different clinicopathologic and computed
803 tomography imaging characteristics of primary and acquired EGFR T790M
804 mutations in patients with non-small-cell lung cancer. *Cancer Manag Res.* 2021;
805 13: 6389-6401.

- 806 101 Jiang M, Zhang Y, Xu J et al. Assessing EGFR gene mutation status in non-small
807 cell lung cancer with imaging features from PET/CT. *Nucl Med Commun.* 2019;
808 40(8): 842-849.
- 809 102 Kawazoe Y, Shiinoki T, Fujimoto K et al. Comparison of the radiomics-based
810 predictive models using machine learning and nomogram for epidermal growth
811 factor receptor mutation status and subtypes in lung adenocarcinoma. *Phys Eng*
812 *Sci Med.* 2023; 46(1): 395-403.
- 813 103 Koyasu S, Nishio M, Isoda H et al. Usefulness of gradient tree boosting for
814 predicting histological subtype and EGFR mutation status of non-small cell lung
815 cancer on (18)F FDG-PET/CT. *Ann Nucl Med.* 2020; 34(1): 49-57.
- 816 104 Li S, Ding C, Zhang H et al. Radiomics for the prediction of EGFR mutation
817 subtypes in non-small cell lung cancer. *Med Phys.* 2019; 46(10): 4545-4552.
- 818 105 Li H, Gao C, Sun Y et al. Radiomics analysis to enhance precise identification of
819 epidermal growth factor receptor mutation based on positron emission
820 tomography images of lung cancer patients. *J Biomed Nanotechnol.* 2021; 17(4):
821 691-702.
- 822 106 Liu Y, Kim J, Balagurunathan Y et al. Radiomic features are associated with
823 EGFR mutation status in lung adenocarcinomas. *Clin Lung Cancer.* 2016; 17(5):
824 441-448.e446.
- 825 107 Liu Z, Zhang T, Lin L et al. Applications of radiomics-based analysis pipeline
826 for predicting epidermal growth factor receptor mutation status. *Biomed Eng*
827 *Online.* 2023; 22(1): 17.
- 828 108 Lu L, Sun SH, Yang H et al. Radiomics prediction of EGFR status in lung
829 cancer-our experience in using multiple feature extractors and The Cancer
830 Imaging Archive Data. *Tomography.* 2020; 6(2): 223-230.
- 831 109 Ruan D, Fang J, Teng X. Efficient 18F-Fluorodeoxyglucose positron emission
832 tomography/computed tomography-based machine learning model for predicting
833 epidermal growth factor receptor mutations in non-small cell lung cancer. *Q J*
834 *Nucl Med Mol Imaging.* 2022.
- 835 110 Trivizakis E, Souglakos J, Karantanas A et al. Deep radiotranscriptomics of non-
836 small cell lung carcinoma for assessing molecular and histology subtypes with a
837 data-driven analysis. *Diagnostics (Basel).* 2021; 11(12).
- 838 111 Yamazaki M, Yagi T, Tominaga M et al. Role of intratumoral and peritumoral
839 CT radiomics for the prediction of EGFR gene mutation in primary lung cancer.
840 *Br J Radiol.* 2022; 95(1140): 20220374.
- 841 112 Yang B, Ji HS, Zhou CS et al. (18)F-fluorodeoxyglucose positron emission
842 tomography/computed tomography-based radiomic features for prediction of
843 epidermal growth factor receptor mutation status and prognosis in patients with
844 lung adenocarcinoma. *Transl Lung Cancer Res.* 2020; 9(3): 563-574.
- 845 113 Zhang J, Zhao X, Zhao Y et al. Value of pre-therapy (18)F-FDG PET/CT
846 radiomics in predicting EGFR mutation status in patients with non-small cell
847 lung cancer. *Eur J Nucl Med Mol Imaging.* 2020; 47(5): 1137-1146.

- 848 114 Zhang T, Liu Z, Lin L et al. Detection of the gene mutation of epidermal growth
849 factor receptor in lung adenocarcinoma by radiomic features from a small
850 amount of PET data. *Nucl Med Commun.* 2023.
- 851 115 Zhao W, Wu Y, Xu Y et al. The potential of radiomics nomogram in non-
852 invasively prediction of epidermal growth factor receptor mutation status and
853 subtypes in lung adenocarcinoma. *Front Oncol.* 2019; 9: 1485.
- 854

Table 1. Methodological characteristics of the studies ($N = 89$) included in the systematic review. For those studies with the same name for the first author and published the same year, a hashtag was added to unequivocally indicate those that were included in the different meta-analyses and consequently, that are represented in the forest plots.

Author-Year	Imaging modality	Contrast-CT*	Tumor segmentation	Model	Classifier (ML)	Datasets			Partition strategy
						Training	Validation	Test	
Agüloğlu et al. 2022 ⁹²	PET/CT	Non-contrast CT	Semi-automatic	ML	RF NB KNN DT SVM LR	133	56	–	Training-Validation split
Aerts et al. 2016 ³⁴	CT	Non-contrast CT	Semi-automatic	Classical statistical model	–	–	–	–	–
Agazzi et al. 2021 ⁹³	CT	Contrast-enhanced	Manual	ML	GBM	104	67	–	Training-Validation split

Aide et al. 2022 ³⁰	PET	–	Manual	ML	LASSO	87	22	–	Training-Validation split
Chang et al. 2021 ^{#49}	PET/CT	Non-contrast CT	Manual	ML	LASSO	409	174	–	Training-Validation split
Chang et al. 2021 ^{##72}	PET/CT	Non-contrast CT	Manual	ML	LR [†]	367	159	–	Training-Validation split
Chen et al. 2021 ⁹⁴	CT	Non-contrast CT	Manual	ML	SVM	179	44	–	Training-Validation split
Chen et al. 2022 ⁹⁵	CT	Non-contrast CT	Semi-automatic	ML	LASSO	176	57	–	Training-Validation split
Choe et al. 2021 ⁹⁶	CT	Contrast-enhanced	Semi-automatic	ML	LR	349	154	–	Training-Validation split
Dang et al. 2021 ¹⁹	CT	Non-contrast CT	Semi-automatic	ML	LASSO	88	30	–	Training-Validation split
Digumarthy et	CT	Contrast-enhanced	Not specified	Classical	–	–	–	–	–

al. 2019 ⁹⁷				statistical model					
Dong et al. 2022 ³³	CT	Non-contrast CT	Not specified	ML	LR	87	45	–	Training-Validation split
Dong et al. 2021 ⁵⁰	CT	Non-contrast CT	Manual	DL ML	RF	363	162	–	Training-Validation split
Feng et al. 2022 ³⁶	CT	Non-contrast CT	Manual	ML	RF XGBoost LR SVM	151	–	–	Training-Validation split
Gao et al. 2023 ⁵¹	PET/CT	Non-contrast CT	Semi-automatic	ML	LR RF SVM	404	111	–	Training-Validation split
Hao et al. 2022 ⁹⁸	CT	Non-contrast CT	Manual	ML	SVM XGBoost AdaBoost LBP DT	154	39	–	Training-Validation split

					LR				
He et al. 2022 ⁹⁹	CT	Non-contrast CT	Semi-automatic	ML	RF KNN LGBM SVM	-	-	-	Training-Validation split
Hong et al. 2020 ²⁴	CT	Contrast-enhanced	Manual	ML	NBC KNN RF SVM DT LR	140	61	-	Training-Validation split
Huang et al. 2018 ³⁵	CT	Non-contrast CT	Semi-automatic	Classical statistical model	-	-	-	-	-
Huang et al. 2022 ⁴⁴	PET/CT	Non-contrast CT	Manual	DL ML	LR	138	57	-	Training-Validation split
Huang et al. 2022 ³⁷	CT	Non-contrast CT	Manual	DL	LR	770	304	-	Training-Validation split

				ML					
Huo et al. 2022 ⁵²	CT	Contrast-enhanced	Manual	ML	GBT	487	121	–	Training-Validation split
Hou et al. 2021 ¹⁰⁰	CT	Contrast-enhanced	Semi-automatic	Classical statistical model	–	144	62	–	Training-Validation split
Jia et al. 2019 ³⁸	CT	Non-contrast CT	Semi-automatic	ML	RF	345	158	–	Training-Validation split
Jiang et al. 2019 ¹⁰¹	PET/CT	Non-contrast CT	Semi-automatic	ML	SVM	–	–	–	10-fold cross-validation
Jiang et al. 2022 ⁵³	CT	Non-contrast CT	Manual	ML	SVM	514	178	–	Training-Validation split
Kawazoe et al. 2023 ⁴⁵	CT	Non-contrast CT	Semi-automatic	ML	SVM LR LGBM	120	44	–	Training-Validation split
Kawazoe et al.	CT	Non-contrast CT	Semi-automatic	ML	SVM	120	52	–	Training-Validation

2023 ¹⁰²					LR				split
Koyasu et al. 2020 ¹⁰³	PET/CT	Non-contrast CT	Manual	ML	RF XGBoost	–	–	–	10-fold cross-validation
Le et al. 2021 ⁵⁴	CT	Non-contrast CT	Manual	ML	XGBoost	143	18	–	Training-Validation split
Li et al. 2018# ⁵⁸	CT	Non-contrast CT	Manual	DL ML	RF	810	200	–	Training-Validation split
Li et al. 2018 ³¹	CT	Contrast-enhanced	Semi-automatic	ML	SVM	–	–	–	3-fold cross-validation
Li et al 2019# ⁵⁷	PET/CT	Non-contrast CT	Manual	ML	Boosting ML scheme	115	–	–	10-fold cross-validation
Li et al. 2019 ¹⁰⁴	CT	Non-contrast CT	Manual	ML	LR	236	76	–	Training-Validation split
Li et al. 2020 ⁵⁶	CT	Non-contrast CT	Manual	ML	LR SVM	326	112	–	Training-Validation split

					RF NB Neural network				
Li et al. 2021 ¹⁰⁵	PET	–	Semi-automatic	ML	SVM	50	25	–	Training-Validation split
Li et al. 2022 ⁵⁵	PET/CT	Non-contrast CT	Manual	ML	LR	125	54	–	Training-Validation split
Liu et al. 2016 ¹⁰⁶	CT	Non-contrast CT	Semi-automatic	Classical statistical model	–	–	–	–	–
Liu et al. 2020 ^{#39}	CT	Contrast-enhanced	Semi-automatic	ML	LR	210	53	–	Training-Validation split
Liu et al. 2020 ²²	PET/CT	Non-contrast CT	Manual	ML	XGBoost	111	37	–	Training-Validation split
Liu et al. 2022 ⁵⁹	CT	Non-contrast CT	Manual	ML	LR DT RF	296	50	–	Training-Validation split

					SVM				
Liu et al. 2023 ¹⁰⁷	PET/CT	Non-contrast CT	Manual	ML	LR DT RF SVM	-	-	-	10-fold cross-validation
Lu et al. 2020 ^{#46}	CT	Non-contrast CT	Manual	ML	LR	83	-	21	Training-Validation split
Lu et al. 2020 ¹⁰⁸	CT	Non-contrast CT	Semi-automatic	ML	KNN Bagging SVM RF	105	228	-	Training-Validation split
Lu et al. 2022 ²⁵	CT	Non-contrast CT	Manual	ML	DT AdaBoost NB RF LR SVM XGBoost	140	61	-	Training-Validation split

					KNN				
Ma et al. 2020 ⁷³	CT	Contrast-enhanced	Manual	ML	SVM	98	42	–	Training-Validation split
Mei et al. 2018 ⁴⁰	CT	Non-contrast CT	Manual	Classical statistical model	–	–	–	–	–
Mu et al. 2020 ⁸⁵	PET/CT	Non-contrast CT	Manual	DL	–	429	187	65	Training-Validation split
Nair et al. 2021 ¹⁷	PET/CT	Contrast-enhanced	Manual	ML	LR	–	–	–	LOOCV
Ninomiya et al. 2021 ⁶⁰	CT	Contrast-enhanced	Manual	ML	SVM	99 [‡]	99 [‡]	95	Training-Validation split
Ninomiya et al. 2023 ⁶¹	CT	Contrast-enhanced	Not specified	ML	SVM	92	62	–	Training-Validation split
Omura et al. 2023 ²⁰	CT	Contrast-enhanced	Automatic	ML	RF	–	–	–	Training-Validation split

Ríos Velázquez et al. 2017 ⁶²	CT	Contrast + Non-contrast CT	Semi-automatic	ML	RF	353	352	–	Training-Validation split
Rossi et al. 2021 ⁶³	CT	Non-contrast CT	Manual	ML	SVM	–	109	61	Training-Validation split
Ruan et al. 2022 ¹⁰⁹	PET/CT	Non-contrast CT	Manual	ML	SVM	70	30	–	Training-Validation split
Shao et al. 2022 ⁹⁰	CT	Non-contrast CT	Semi-automatic	DL	–	–	–	–	Training-Validation split
Shiri et al. 2020 ¹⁸	CT low dose CTD PET/CT	Contrast-enhanced	Manual Automatic [§]	ML	SVM KNN DT QDA MLP SGD LR NB GNB	82	68	–	10-fold cross-validation

					RF AdaBoost Bagging				
Shiri et al. 2022 ⁸⁸	PET/CT	Non-contrast CT	Manual Automatic [§]	ML	RF	-	-	-	Training-Validation split
Song et al. 2021 ⁴²	CT	Not specified	Manual Automatic	DL ML	SVM	528	137	-	Training-Validation split
Song et al. 2020 ⁷⁴	CT	Non-contrast CT	Automatic	ML	DT	268	67	-	Training-Validation split
Trivizakis et al. 2021 ¹¹⁰	CT	Not specified	Not specified	DL ML	KNN DT RBF-GPC RBF-SVM Linear SVM Polynomial SVM Sigmoid SVM	-	-	-	5-fold cross-validation

Tu et al. 2019 ⁶⁴	CT	Non-contrast CT	Not specified	ML	LR	243	161	–	Training-Validation split
Wang et al. 2019 ²¹	CT	Contrast-enhanced	Manual	ML	SVM	41	–	–	Training-Validation split
Wang et al. 2021 ⁴³	CT	Non-contrast CT	Manual	DL	–	882	125	255	Training-Validation split
Wang et al. 2022 ^{#65}	CT	Non-contrast CT	Manual	DL ML	LASSO	–	–	–	Training-Validation split [¶]
Wang et al. 2022 ^{##47}	PET/CT	Non-contrast CT	Semi-automatic	ML	LR	180	78	–	Training-Validation split
Weng et al. 2021 ⁶⁶	CT	Non-contrast CT	Semi-automatic	ML	LR	210	91	–	Training-Validation split
Wu et al. 2020 ²⁶	CT	Contrast-enhanced	Manual	ML	LR	–	–	–	10-fold cross-validation
Xiao et al.	PET/CT	Non-contrast CT	Manual	DL	RF	121	29	–	Training-Validation

2023 ⁹¹				ML					split
Yamazaki et al. 2022 ¹¹¹	CT	Non-contrast CT	Semi-automatic	ML	RF	-	-	-	-
Yang et al. 2020 ^{#27}	CT	Contrast-enhanced	Semi-automatic	ML	LASSO	130	40	-	Training-Validation split
Yang et al. 2020 ¹¹²	PET/CT	Non-contrast CT	Semi-automatic	ML	RF	139	35	-	Training-Validation split
Yang et al. 2022 ^{#67}	CT	Contrast + Non-contrast CT	Manual	ML	LR RF SVM GBT NB	327	66	19	Training-Validation split
Yang et al. 2022 ²³	PET/CT	Non-contrast CT	Semi-automatic	ML	SVM DT RF	218	95	-	Training-Validation split
Yang et al.	CT	Contrast-enhanced	Manual	ML	LR	176	74	-	Training-Validation

2022 ⁴⁸									split
Yip et al. 2017 ⁸⁹	PET	-	Manual	Classical statistical model	-	-	-	-	-
Zhang et al. 2018 ²⁸	CT	Non-contrast CT	Manual	ML	LR	140	40	-	Training-Validation split
Zhang et al. 2020 ^{#70}	PET/CT	Non-contrast CT	Manual	ML	RF SVM LR	-	-	-	10-fold cross-validation
Zhang et al. 2020 ¹¹³	PET/CT	Non-contrast CT	Semi-automatic	ML	LR	175	73	-	Training-Validation split
Zhang et al. 2020 ^{##68}	CT	Non-contrast CT	Semi-automatic	DL ML	RF SVM	638	71	205	Training-Validation split
Zhang et al.	CT	Contrast-enhanced	Semi-automatic	ML	LASSO	-	-	-	Training-Validation

2021 ⁴¹									split
Zhang et al. 2021 ⁶⁹	CT	Non-contrast CT	Manual	ML	DT LR SVM Multivariate analysis for C- R-R model	294	126	-	Training-Validation split
Zhang et al. 2023 ¹¹⁴	PET	-	Manual	ML	SVM RF LR AdaBoost	-	-	-	10-fold cross- validation
Zhao et al. 2019 ⁸⁶	CT	Non-contrast CT	Manual	DL ML	LR	348	116	116	Training-Validation split
Zhao et al. 2019 ¹¹⁵	CT	Non-contrast CT	Manual	ML	LR	322	315	-	Training-Validation split
Zhao et al. 2022 ⁷¹	PET/CT	Non-contrast CT	Semi-automatic	ML	LR	65	23	-	Training-Validation split

Zhu et al. 2022 ³²	CT	Non-contrast CT	Semi-automatic	ML	LASSO RF SVM	875	217	–	Training-Validation split
Zhu et al. 2021 ²⁹	CT	Contrast-enhanced	Manual	ML	SVM KNN RF LR	159	40	–	Training-Validation split
Zuo et al. 2023 ⁸⁷	PET/CT	Non-contrast CT	Manual	ML	LGBM XGBoost RF LR	410	170	180	Training-Validation split

*In studies in which PET/CT was performed, only details about contrast were provided for PET acquisition. Consequently, it was assumed that CT scans were non-contrast enhanced.

†Not specified but inferred from the methodology and results.

‡Number of cases for training and validation sets not specified; only a total number for both cohorts provided.

§Manual segmentation for PET images; automatic segmentation for CT images.

¶80% Training-Validation split.

CT, computed tomography; CTD, contrast-enhanced diagnostic quality; DL, deep learning; DT, decision tree; ERBB2, v-erb-b2 avian erythroblastic leukemia viral oncogene homolog 2;

GBM, gradient boosted machine; GBT, gradient boosting tree; GNB, Gaussian Naives Bayes; GPC, Gaussian processes classification; LASSO, least absolute shrinkage and selection operator; LBP, local binary pattern; LGBM, Light gradient boosted machine; LOOCV, leave-one-out cross-validation; LR, logistic regression; ML, machine learning; MLP, multilayer perceptron; NB, Naive Bayes; KNN, K-nearest neighbors; PET, positron emission tomography; QDA, quadratic discriminant analysis; RBF, radial basis function; RF, random forest; SGD, stochastic gradient descent; SVM, support vector machine; TP53, tumor suppressor protein 53.

Table 2. Clinical characteristics of the studies ($N = 89$) included in the systematic review. For those studies with the same name for the first author and published the same year, a hashtag was added to unequivocally indicate those that were included in the different meta-analyses and consequently, that are represented in the forest plots.

Author-Year	Target oncogene mutation	Design	Total of patients	Sex		Age Mean/median	Histology	Smoking status		TNM stage	Treatment
				Female	Male			Current /former smoker	Non-smoker		
Agüloğlu et al. 2022 ⁹²	EGFR ALK	Unicentric	189	59	130	62/-	NSCLC	130	59	Stages I-IV	Naïve
Aerts et al. 2016 ³⁴	EGFR	Unicentric	47	-	-	-/-	NSCLC	-	-	-	Naïve + post-treatment images
Agazzi et al. 2021 ⁹³	EGFR ALK	Unicentric	84	39	45	-/63	ADC	57	27	-	Naïve
Aide et al. 2022 ³⁰	EGFR	Unicentric	109	34	75	-/66	ADC	96	13	Stages II-IV	Naïve

Chang et al. 2021 ^{#49}	EGFR	Unicentric	583	305	278	-/62	ADC	229	354	Stages I-III	Naïve
Chang et al. 2021 ^{##72}	ALK	Unicentric	526	272	254	-/58.25	ADC	202	324	Stages I-IV	Naïve
Chen et al. 2021 ⁹⁴	EGFR	Unicentric	223	109	114	64.63/-	NSCLC	55	168	Stages I-IV	Naïve
Chen et al. 2022 ⁹⁵	EGFR	Unicentric	233	105	128	57.5/-	ADC	65	168	Stages I-IV	Naïve
Choe et al. 2021 ⁹⁶	ALK	Unicentric	503	273	230	62.5/-	ADC	200	303	Stages I-IV	Not specified
Dang et al. 2021 ¹⁹	EGFR	Not specified	118	55	63	63.82/-	ADC, SCC	-	-	Stages I-III	No treatment*
Digumarthy et al. 2019 ⁹⁷	EGFR	Unicentric	93	50	43	60/-	ADC, SCC	61	32	-	Naïve
Dong et al. 2022 ³³	EGFR	Multicentric	132	64	68	58.8/-	NSCLC	42	90	Stages I-III	Naïve
Dong et al.	EGFR	Multicentric	525	250	275	-/65.5	NSCLC	373	152	-	Not specified

2021 ⁵⁰	KRAS										
Feng et al. 2022 ³⁶	EGFR	Multicentric	168	–	–	–/–	NSCLC	–	–	–	Not specified [†]
Gao et al. 2023 ⁵¹	EGFR	Unicentric	515	264	251	64/–	ADC	175	–	Stages I-IV	Naïve
Hao et al. 2022 ⁹⁸	ALK	Unicentric	193	102	91	54.26/–	NSCLC	49	144	Stages II and IV	Naïve
He et al. 2022 ⁹⁹	EGFR	Multicentric	758	317	441	55.6/–	NSCLC	358	400	Stages I-IV	Naïve
Hong et al. 2020 ²⁴	EGFR	Unicentric	201	94	107	58.12/–	ADC	64	137	Stages I-IV	Naïve
Huang et al. 2018 ³⁵	EGFR	Unicentric	46	–	–	–/–	NSCLC	–	–	–	Naïve + post-treatment images
Huang et al. 2022 ⁴⁴	EGFR	Unicentric	195	72	123	61.14 –	NSCLC	127	68	–	No treatment*
Huang et al. 2022 ³⁷	EGFR	Unicentric	1074	–	–	–/–	NSCLC	–	–	–	Not specified

Huo et al. 2022 ⁵²	EGFR	Unicentric	608	272	336	61.7/-	ADC	0	335	Stages II and IV	Naïve
Hou et al. 2021 ¹⁰⁰	EGFR	Unicentric	206	120	86	-/59	ADC, SCC, ASC [‡]	57	-	Stages I-IV	Naïve
Jia et al. 2019 ³⁸	EGFR	Unicentric	503	249	254	-/60.5	ADC	80	423	Stages I-IV	Not specified [†]
Jiang et al. 2019 ¹⁰¹	EGFR	Unicentric	80	32	48	64/62.5	NSCLC	21	59	-	Naïve
Jiang et al. 2022 ⁵³	EGFR	Unicentric	692	-	-	59/-	ADC	-	-	-	Naïve
Kawazoe et al. 2023 ⁴⁵	EGFR	Unicentric	164	75	89	70.24/-	ADC	102	62	Stages I-IV	No treatment [§]
Kawazoe et al. 2023 ¹⁰²	EGFR	Unicentric	172	77	95	70.76/-	ADC	107	65	Stages I-IV	Naïve
Koyasu et al. 2020 ¹⁰³	EGFR	Unicentric	138	54	84	67.8/-	ADC, SCC	-	-	-	Not specified

Le et al. 2021 ⁵⁴	EGFR KRAS	Multicentric	161	50	111	68.05/–	ADC, NSCLC NOS, SCC	61	100	–	Naïve
Li et al. 2018 ^{#58}	EGFR	Unicentric	1010	457	553	–/63	ADC	262	748	Stages I-IV	Naïve
Li et al. 2018 ³¹	EGFR	Unicentric	51	19	32	58.1/–	ADC	24	27	Stages I-III	Not specified [†]
Li et al 2019 ^{#57}	EGFR	Unicentric	115	62	53	–/63	NSCLC	36	79	Stages II and IV	Naïve
Li et al. 2019 ¹⁰⁴	EGFR	Unicentric	312	164	148	Freq./Freq. [‡]	ADC, SCC	109	203	Stages II and IV	Naïve
Li et al. 2020 ⁵⁶	EGFR	Multicentric	438	–	–	61.31/–	ADC	–	–	–	Naïve
Li et al. 2021 ¹⁰⁵	EGFR	Unicentric	75	45	30	62/–	Lung cancer ^{**}	34	41	–	Not specified
Li et al. 2022 ⁵⁵	EGFR	Unicentric	179	103	76	61.51/59.5	ADC	65	114	–	Naïve
Liu et al. 2016 ¹⁰⁶	EGFR	Unicentric	298	172	126	–/60	ADC, Others	136	162	Stages II and IV	Naïve

Liu et al. 2020 ^{#39}	EGFR	Unicentric	263	121	142	62.5/-	ADC	31	232	-	Not specified [†]
Liu et al. 2020 ²²	EGFR	Unicentric	148	63	85	-/61.2	ADC	-	-	Stages II-IV	Naïve
Liu et al. 2022 ⁵⁹	EGFR	Multicentric	346	141	205	66.69/-	ADC, SCC, LCC, PSC	225	121	-	Naïve
Liu et al. 2023 ¹⁰⁷	EGFR	Unicentric	115	62	53	-/62.75	ADC	36	79	Stages I-IV	Naïve
Lu et al. 2020 ^{#46}	EGFR	Unicentric	104	64	40	58.27/-	ADC	30	74	Stages I-IV	No treatment*
Lu et al. 2020 ¹⁰⁸	EGFR	Multicentric	228 ^{††}	85 ^{††}	120 ^{††}	67.94/-	ADC, SCC, NOS	-	-	Stages 0-IV	Not specified
Lu et al. 2022 ²⁵	EGFR	Unicentric	201	99	102	64.81/-	ADC	84	117	Stages III-IV	Naïve
Ma et al. 2020 ⁷³	ALK	Unicentric	140	87	53	54.19/-	ADC	45	95	Stages II and IV	Naïve
Mei et al. 2018 ⁴⁰	EGFR	Unicentric	296	144	152	58.56/-	ADC	86	210	-	Not specified [†]

Mu et al. 2020 ⁸⁵	EGFR	Multicentric	681	303	378	61,83/–	ADC, SCC	315	366	Stages I-IV	Naïve
Nair et al. 2021 ¹⁷	EGFR	Unicentric	50	18	32	–/–	NSCLC	35	15	–	Naïve
Ninomiya et al. 2021 ⁶⁰	EGFR	Multicentric	194	74	120	–/67	NSCLC	128	66	Stages I-IV	Not specified
Ninomiya et al. 2023 ⁶¹	EGFR	Multicentric	154	86	68	–/67	Lung cancer	73	81	Stages I-IV	Not specified
Omura et al. 2023 ²⁰	EGFR	Unicentric	99	65	34	66/–	ADC	41	–	Stages I-II	Naïve
Ríos Velázquez et al. 2017 ⁶²	EGFR KRAS	Multicentric	763	459	304	65/–	ADC	548	215	Stages I-IV	Not specified
Rossi et al.	EGFR	Multicentric	170	–	–	–/–	ADC	110	30	–	Naïve

2021 ⁶³											
Ruan et al. 2022 ¹⁰⁹	EGFR	Unicentric	100	42	58	– / 64.5	NSCLC	33	67	Stages I-IV	Naïve
Shao et al. 2022 ⁹⁰	EGFR	Unicentric	1096	–	–	58.26/–	NSCLC	–	–	–	Naïve
Shiri et al. 2020 ¹⁸	EGFR KRAS	Unicentric	150	–	–	69.1 –	ADC, SCC, NOS [‡]	–	–	–	Not specified
Shiri et al. 2022 ⁸⁸	EGFR KRAS	Multicentric	136	–	–	–/–	ADC, SCC, NOS	–	–	–	Not specified
Song et al. 2021 ⁴²	EGFR	Multicentric	665	336	329	Freq./Freq. [¶]	ADC	334	331	Stages II and IV	Not specified ^{**}
Song et al. 2020 ⁷⁴	ALK	Unicentric	335	196	139	57 / –	ADC	103	232	Stages I-IV	Naïve

Trivizakis et al. 2021 ¹¹⁰	EGFR	Unicentric	112	–	–	–/–	ADC, SCC	–	–	–	Not specified
Tu et al. 2019 ⁶⁴	EGFR	Unicentric	404	211	193	59.95/–	NSCLC	114	290	Stages II and IV	Naïve
Wang et al. 2019 ²¹	EGFR	Unicentric	51	35	16	58.45/–	ADC	9	42	Stages 0-II	Not specified
Wang et al. 2021 ⁴³	EGFR PD-L1	Unicentric	1262	642	620	57.7/–	ADC, SCC, Others [‡]	452	749	Stages I-IV	Not specified ^{§§}
Wang et al. 2022 ^{#65}	EGFR PD-L1	Unicentric	3629	1674	1955	59.29/–	ADC, SCC, Others	1413	1981	Stages I-IV	Naïve
Wang et al. 2022 ^{##47}	KRAS	Unicentric	258	78	180	62.35/–	NSCLC	166	92	–	No treatment*
Weng et al. 2021 ⁶⁶	EGFR	Unicentric	301	145	156	64.95/–	NSCLC	110	191	–	Naïve

Wu et al. 2020 ²⁶	EGFR	Unicentric	67	29	38	56.35/-	ADC, SCC	34	33	Stages III-IV	Naïve
Xiao et al. 2023 ⁹¹	EGFR	Unicentric	150	59	91	-/58	NSCLC	64	86	-	Not specified
Yamazaki et al. 2022 ¹¹¹	EGFR	Unicentric	478	190	288	Freq./Freq. [¶]	ADC, SCC, Others [‡]	-	-	Stages II and IV	Naïve
Yang et al. 2020 ^{#27}	EGFR	Unicentric	253	155	98	-/62	ADC	105	148	Stages III-IV	Naïve
Yang et al. 2020 ¹¹²	EGFR	Unicentric	174	81	93	61.72/-	ADC	59	115	Stages II and IV	Naïve
Yang et al. 2022 ^{#67}	EGFR	Unicentric	412	223	189	62/-	ADC, SCC	105	307	-	Naïve
Yang et al. 2022 ²³	EGFR	Unicentric	313	164	149	59.21/-	ADC	105	208	Stages II-IV	Naïve
Yang et al. 2022 ⁴⁸	EGFR	Unicentric	250	-	-	56.35 / -	ADC	-	-	-	Treated with TKIs ^{¶¶}

Yip et al. 2017 ⁸⁹	KRAS	Unicentric	348	214	134	–/65	ADC, NSCLC NOS, SC. Not available for 1 patient [‡]	286	62	Stages I-IV	Naïve
Zhang et al. 2018 ²⁸	EGFR	Unicentric	180	46	134	59.7/–	ADC, SCC, Others	119	61	Stages III-IV	Naïve
Zhang et al. 2020# ⁷⁰	EGFR	Unicentric	173	58	115	60.8/–	ADC SCC, LCC, NSCLC- NOS	–	–	Stages I-IV	Naïve
Zhang et al. 2020 ¹¹³	EGFR	Unicentric	248	113	135	62.23/–	ADC	117	131	Stages I-IV	Naïve
Zhang et al. 2020## ⁶⁸	EGFR	Unicentric	914	493	421	59.79/–	ADC	–	–	–	Naïve

Zhang et al. 2021 ⁴¹	EGFR KRAS ERBB2 TP53	Unicentric	134	56	78	63.6/-	ADC, SCC, ASC	28	106	-	Not specified
Zhang et al. 2021 ⁶⁹	EGFR	Unicentric	420	201	219	57.43/56.5	ADC	147	273	-	Naïve
Zhang et al. 2023 ¹¹⁴	EGFR	Unicentric	115	-	-	-/-	NSCLC	-	-	-	Naïve
Zhao et al. 2019 ⁸⁶	EGFR	Unicentric	579	334	245	60.1/-	ADC	-	-	Stages 0-IV	Not specified
Zhao et al. 2019 ¹¹⁵	EGFR	Unicentric	637	368	269	59.9/-	ADC	49	588	-	Naïve
Zhao et al. 2022 ⁷¹	EGFR	Unicentric	88	39	49	64.23/-	ADC	31	57	Stages II and IV	Naïve
Zhu et al. 2022 ³²	EGFR	Unicentric	1092	648	442	59.59/-	ADC	-	-	Stages I-III	Naïve

Zhu et al. 2021 ²⁹	EGFR TP53	Unicentric	199	86	113	Freq./Freq. [¶]	ADC	94	105	Stages III-IV	Naïve
Zuo et al. 2023 ⁸⁷	EGFR	Multicentric	767	372	395	-/62.04	ADC	-	-	Stages I-IV Others (34 patients)	Not specified

*Patients were excluded if treated with RT or chemotherapy, but targeted therapy is not specified.

†CT scans acquired prior surgery; no information on prior treatments.

‡Mainly adenocarcinoma cases.

§Patients did receive target treatment, but no information on the administration of other treatments (immunotherapy and/or chemotherapy) is specified.

¶These studies provide age data as frequencies establishing an age threshold.

**Inferred that NSCLC patients were included as it is specified that 17 patients had 19Del and 20 cases had L858R mutation; EGFR mutations are very rare in SCLC.

††In this study, there are 23 patients with no information about sex.

‡‡Image acquired 3 months before PCR; no information about treatments.

§§CT images acquired within 1 month before pathological diagnosis.

¶¶ Imaging-proven progression on first- or second-generation TKIs; patients underwent chest contrast-enhanced CT at the time of confirmed progression, and the interval between CT and confirmed progression was within 3 days.

ADC, adenocarcinoma; ALK, anaplastic lymphoma kinase; ASC, adenosquamous carcinoma; CT, computed tomography; EGFR, epidermal growth factor receptor; ERBB2, v-erb-b2 avian erythroblastic leukemia viral oncogene homolog 2; Freq. , frequency; KRAS, Kirsten rat sarcoma viral oncogene homologue; LCC, large cell lung carcinoma; NOS, not otherwise specified; NSCLC, non-small cell lung cancer; PCR, polymerase chain reaction; PD-L1, programmed death ligand 1; PSC, pulmonary sarcomatoid carcinoma; RT, radiotherapy; SCC, Squamous cell carcinoma; SCLC, small-cell lung cancer; TKI , tyrosine kinase inhibitor; TP53, tumor suppressor protein 53.

FIGURES

Figure 1. PRISMA flowchart. AI, artificial intelligence; CLAIM, Checklist for Artificial Intelligence in Medical Imaging; CT, computed tomography; MRI, magnetic resonance imaging.

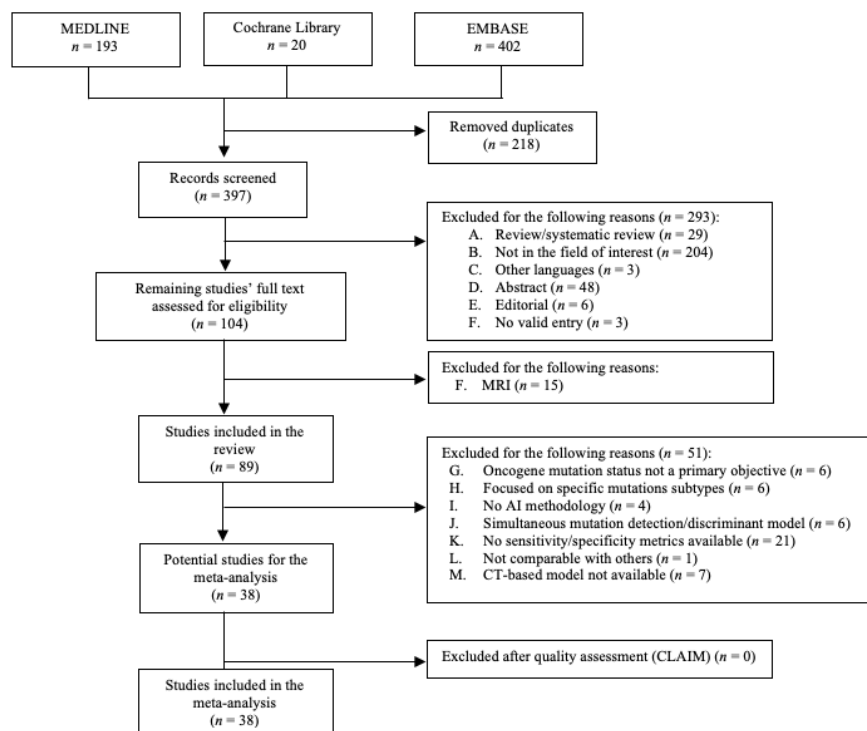
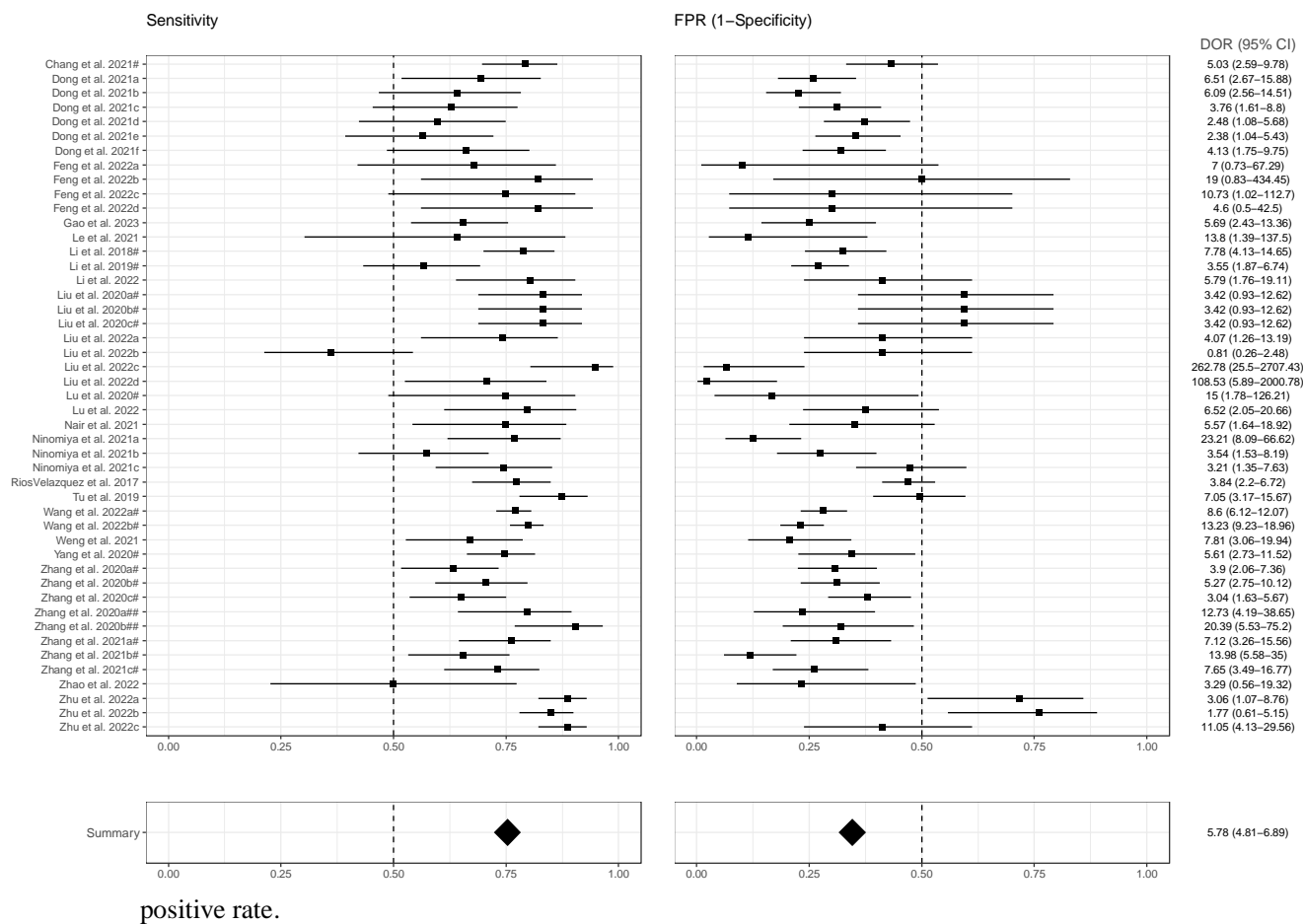


Figure 2. Forest plots of the included studies developing radiomics models using machine learning and/or deep learning methods for the prediction of EGFR mutation status. Numbers are estimated with 95% CIs in brackets and indicated by horizontal lines. For those studies with the same name for the first author and published the same year, a hashtag was added to unequivocally tag them as done in Tables 1 and 2 and in the reference list. EGFR, epidermal growth factor receptor; CI, confidence interval; DOR, diagnostic odds ratio; FPR, false



positive rate.

Figure 3. Forest plots of the included studies developing combined models (radiomics + clinical data) using machine learning and/or deep learning methods for the prediction of EGFR mutation status. Numbers are estimates with 95% CIs in brackets and indicated by horizontal lines. For those studies with the same name for the first author and published the same year, a hashtag was added to unequivocally tag them as done in Tables 1 and 2 and in the reference list. EGFR, epidermal growth factor receptor; CI, confidence interval; DOR, diagnostic odds ratio;

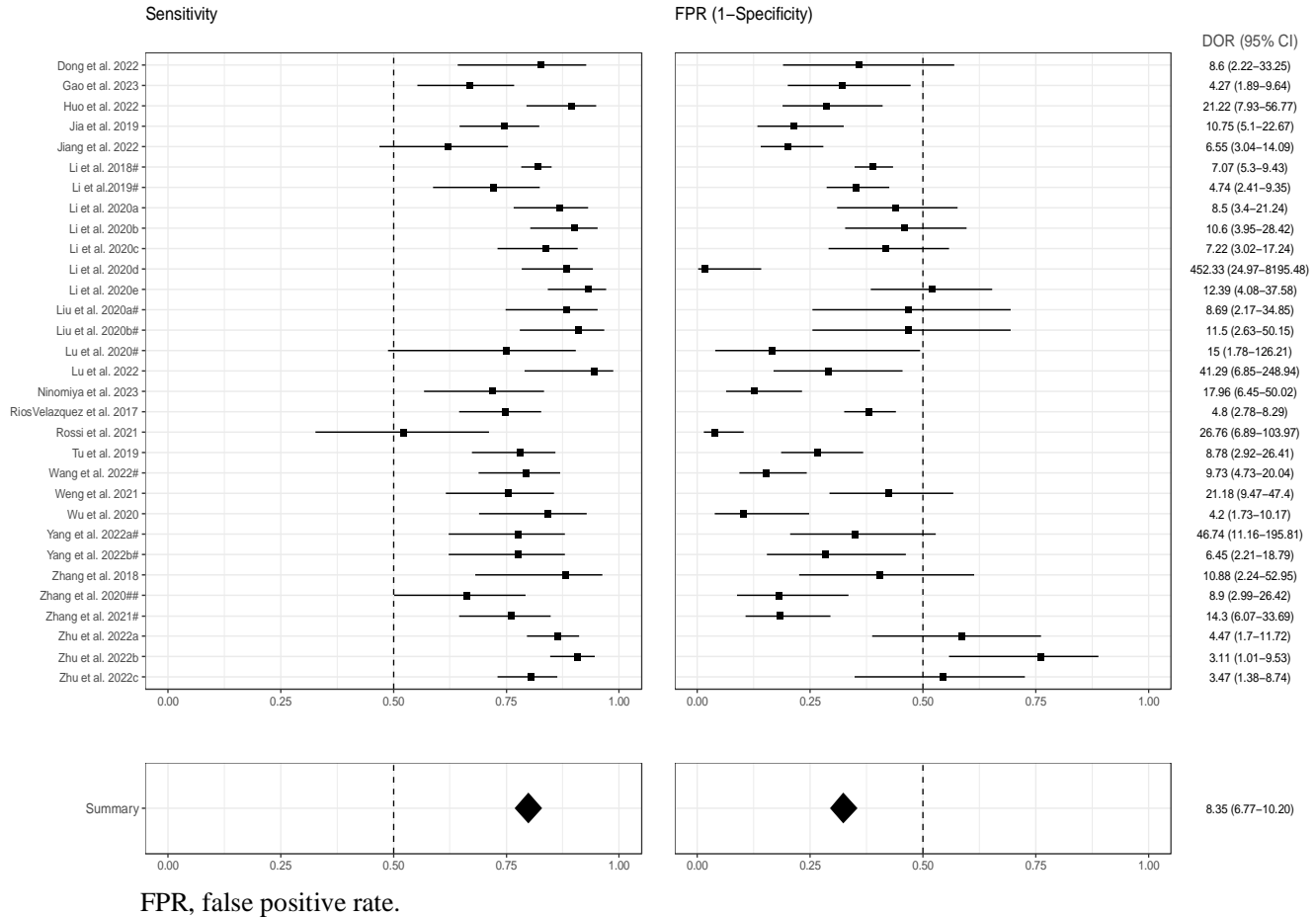
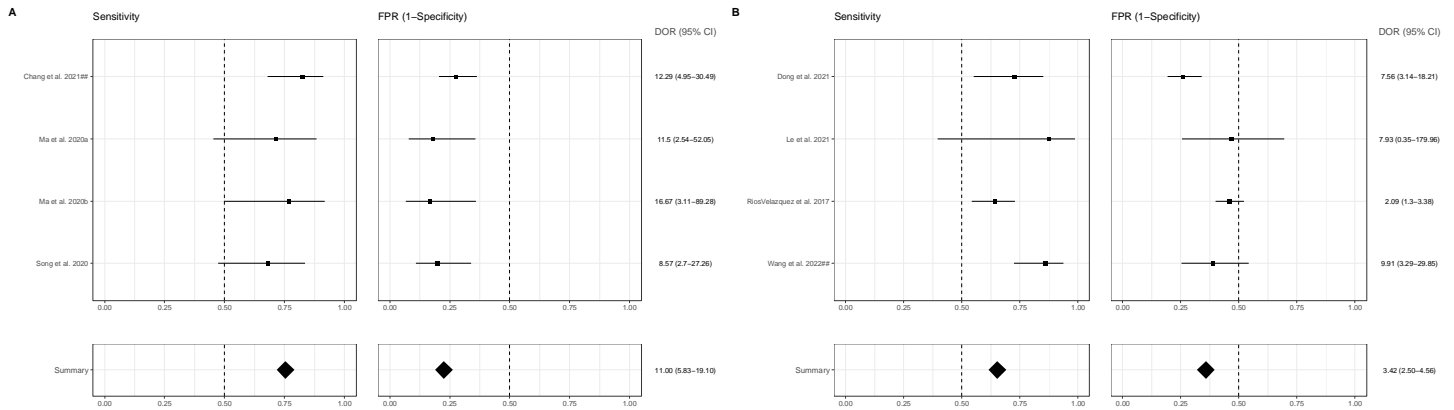
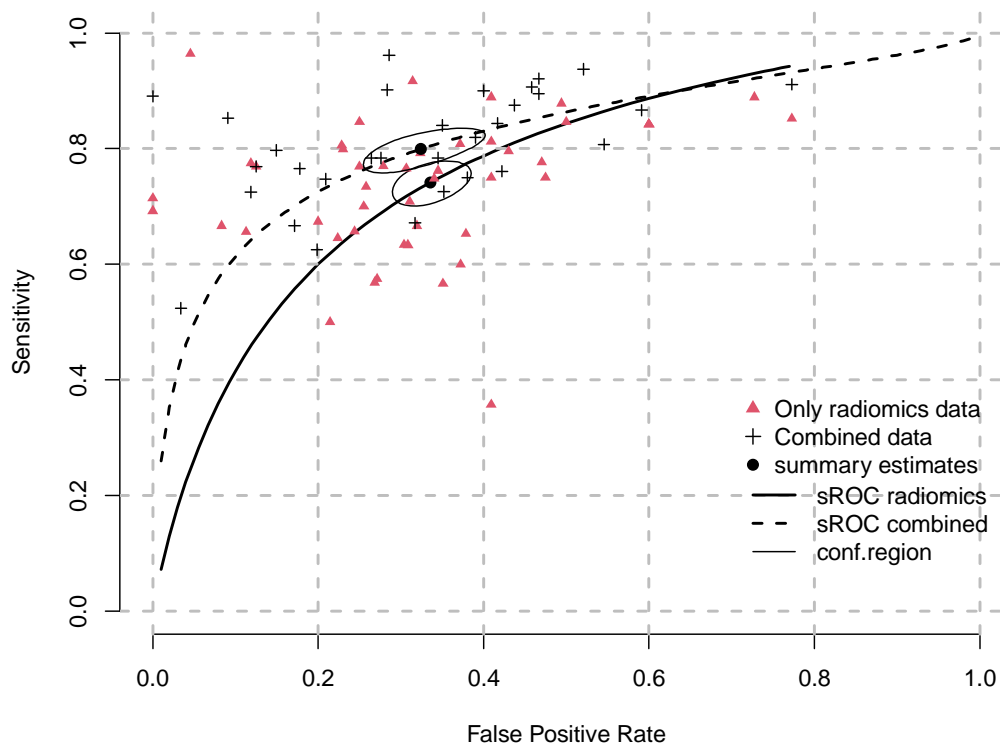


Figure 4. Forest plots of the included studies developing radiomics models using machine learning and/or deep learning methods for the prediction of **A) ALK** and **B) KRAS** mutation status. Numbers are estimates with 95% CIs in brackets and indicated by horizontal lines. For those studies with the same name for the first author and published the same year, a hashtag was added to unequivocally tag them as done in Tables 1 and 2 and in the reference list. ALK, anaplastic lymphoma kinase; CI, confidence interval; DOR, diagnostic odds ration; FPR, false

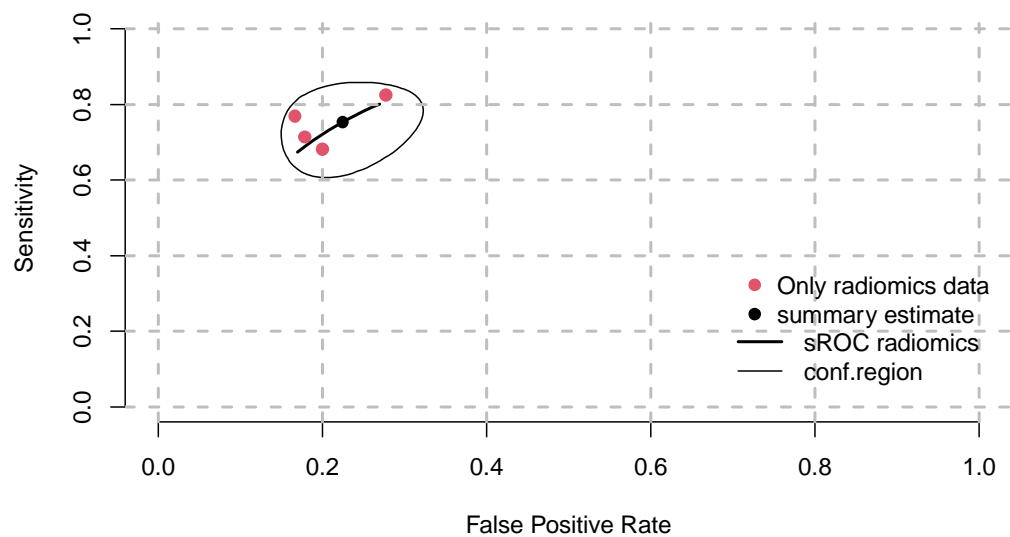


positive rate; KRAS, Kirsten rat sarcoma viral oncogene homologue.

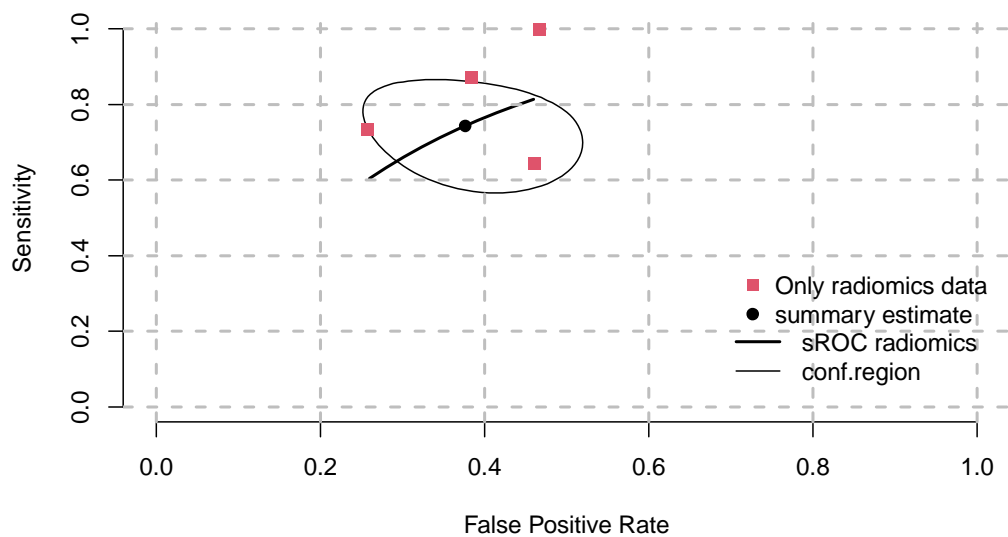
Supplementary Figure S1. Hierarchical sROC curves of included studies for the comparative performance of radiomics models and combined models (radiomics + clinical data) using machine learning and/or deep learning methods for the prediction of EGFR mutation status ($n = 24$ and $n = 23$ studies, respectively). EGFR, epidermal growth factor receptor.



Supplementary Figure S2. Hierarchical sROC curve of included studies for the performance of radiomics models for the prediction of ALK mutation status ($n = 3$). ALK, anaplastic lymphoma kinase.



Supplementary Figure S3. Hierarchical sROC curve of included studies for the performance of radiomics models for the prediction of KRAS mutation status ($n = 4$). KRAS, Kirsten rat sarcoma viral oncogene homologue.



Supplementary tables

Supplementary Table S1. Search strategy applied for the qualitative analysis (systematic review).

Databases	Search strategy
MEDLINE (via Pubmed)	("radiomics"[TIAB] OR "radiomic"[TIAB] OR "texture analysis"[TIAB]) AND ("lung neoplasms"[MESH] OR "lung cancer"[TIAB] OR "NSCLC"[TIAB] or "non-small cell lung cancer"[TIAB] OR "lung adenocarcinoma"[TIAB]) AND ("mutational status" OR "mutation" OR "molecular subtype" OR "ALK"[TIAB] OR "anaplastic lymphoma kinase"[TIAB] OR "BRAF"[TIAB] OR "EGFR"[TIAB] OR "Epidermal growth factor receptor"[TIAB] OR "ERRB2"[TIAB] OR "Receptor, ErbB-2"[MESH] OR "HER2"[TIAB] OR "KRAS"[TIAB] OR "Kirsten rat sarcoma virus"[TIAB] OR "Proto Oncogene Proteins c met"[TIAB] OR "NTRK"[TIAB] OR "ROS"[TIAB] OR "c-ros"[TIAB])
COCHRANE LIBRARY	("radiomics" OR "radiomic" OR "texture analysis") AND ("lung neoplasms" OR "lung cancer" OR "NSCLC" OR "non-small cell lung cancer") AND ("mutational status" OR "mutation" OR "molecular subtype" OR "ALK" OR "anaplastic lymphoma kinase" OR "BRAF" OR "EGFR" OR "ERRB2" OR "Receptor, ErbB-2" OR "HER2" OR "KRAS" OR "Kirsten rat sarcoma virus" OR "Proto Oncogene Proteins c met" OR "NTRK" OR "ROS" OR "c-ros")
EMBASE	('radiomics':ab,ti OR 'radiomics'/exp OR 'radiomic':ab,ti OR 'texture analysis':ab,ti) AND ('lung cancer'/exp OR 'lung cancer':ab,ti OR 'NSCLC'/exp OR 'NSCLC':ab,ti OR 'non small cell lung cancer'/exp OR 'non small cell lung cancer':ab,ti OR 'lung adenocarcinoma'/exp OR 'lung adenocarcinoma':ab,ti) AND

	<p>('mutational status':ab,ti OR ('mutational' NEAR/2 'status') OR 'mutation':ab,ti OR 'mutation'/exp OR 'molecular subtype':ab,ti OR ('molecular' NEAR/2 'subtype') OR 'ALK':ab,ti OR 'ALK gene'/exp OR 'anaplastic lymphoma kinase':ab,ti OR 'anaplastic lymphoma kinase'/exp OR 'BRAF':ab,ti OR 'BRAF gene'/exp OR 'EGFR':ab,ti OR 'EGFR gene'/exp OR 'Epidermal growth factor receptor':ab,ti OR 'Epidermal growth factor receptor gene'/exp OR 'ERRB2':ab,ti OR 'ERRB2 gene'/exp OR 'epidermal growth factor receptor 2'/exp OR 'epidermal growth factor receptor 2':ab,ti OR 'HER2':ab,ti OR 'KRAS':ab,ti OR 'KRAS gene'/exp OR 'Kirsten rat sarcoma virus':ab,ti OR 'Kirsten rat sarcoma virus'/exp OR 'Proto Oncogene Proteins c met' OR 'MET':ab,ti OR 'MET gene'/exp OR 'NTRK':ab,ti OR 'NTRK gene'/exp OR 'c ros oncogene 1':ab,ti OR 'ROS1':ab,ti OR 'ROS1 gene'/exp)</p>
--	---

Supplementary Table S2. Quality assessment results obtained after CLAIM evaluation.

<i>N</i>	Study	Score			Mean score	Cut-off
		Reviewer 1 (A.J.P.)	Reviewer 2 (F.B.B.)	Reviewer 3 (A.P.P.)		
1	Chang et al. 2021 ¹	28	24	27	26	17
2	Chang et al. 2021 ²	26	25	26	26	17
3	Dong et al. 2021 ³	23	22	19	21	18
4	Dong et al. 2022 ⁴	25	22	21	23	18
5	Feng et al. 2022 ⁵	20	22	23	22	18.5
6	Gao et al. 2023 ⁶	22	22	20	21	17.5
7	Huo et al. 2022 ⁷	22	25	25	24	17.5
8	Jia et al. 2019 ⁸	19	19	20	19	17
9	Jiang et al. 2022 ⁹	24	23	22	23	16.5
10	Le et al. 2021 ¹⁰	22	20	21	21	17.5
11	Li et al. 2018 ¹¹	25	28	22	25	19
12	Li et al. 2019 ¹²	23	22	21	22	17
13	Li et al. 2020 ¹³	25	23	22	23	19
14	Li et al. 2022 ¹⁴	21	21	21	21	17

15	Liu et al. 2020 ¹⁵	22	25	23	23	17
16	Liu et al. 2022 ¹⁶	24	23	22	23	17
17	Lu et al. 2020 ¹⁷	27	30	26	28	17.5
18	Lu et al. 2022 ¹⁸	22	25	21	23	17.5
19	Ma et al. 2020 ¹⁹	24	26	22	24	17
20	Nair et al. 2021 ²⁰	21	22	19	21	17.5
21	Ninomiya et al. 2021 ²¹	21	22	21	21	17.5
22	Ninomiya et al. 2023 ²²	21	22	22	22	17
23	Rios Velazquez et al. 2017 ²³	19	23	20	21	18
24	Rossi et al. 2021 ²⁴	20	22	19	20	17.5
25	Song et al. 2020 ²⁵	27	28	27	27	19
26	Tu et al. 2019 ²⁶	19	21	20	20	17
27	Wang et al. 2022 ²⁷	23	26	26	25	18
28	Wang et al. 2022 ²⁸	24	22	22	23	19
29	Weng et al. 2021 ²⁹	24	25	24	24	17.5
30	Wu 2020 ³⁰	20	22	21	21	17
31	Yang 2020 ³¹	22	23	23	23	17
32	Yang 2022 ³²	19	18	18	18	17
33	Zhang 2018 ³³	26	27	23	25	17
34	Zhang 2020 ³⁴	19	19	19	19	17

35	Zhang 2020 ³⁵	22	23	23	23	17
36	Zhang 2021 ³⁶	27	26	26	26	17
37	Zhao 2022 ³⁷	23	24	23	23	19
38	Zhu 2022 ³⁸	22	22	20	21	17.5

Supplementary Table S3. Studies included in the different meta-analyses conducted.

N	EGFR		ALK	KRAS
	Radiomics models	Combined models	Radiomics models	Radiomics models
1	Chang et al. 2021 ¹	Dong et al. 2022 ⁴	Chang et al. 2021 ²	Dong et al. 2021 ³
2	Dong et al. 2021 ³	Gao et al. 2023 ⁶	Ma et al. 2020 ¹⁹	Le et al. 2021 ¹⁰
3	Feng et al. 2022 ⁵	Huo et al. 2022 ⁷	Song et al. 2020 ²⁵	RiosVelazquez et al. 2017 ²³
4	Gao et al. 2023 ⁶	Jia et al. 2019 ⁸		Wang et al. 2022 ²⁸
5	Le et al. 2021 ¹⁰	Jiang et al. 2022 ⁹		
6	Li et al. 2018 ¹¹	Li et al. 2018 ¹¹		
7	Li et al. 2019 ¹²	Li et al. 2019 ¹²		
8	Li et al. 2022 ¹⁴	Li et al. 2020 ¹³		

9	Liu et al. 2020 ¹⁵	Liu et al. 2020 ¹⁵		
10	Liu et al. 2022 ¹⁶	Lu et al. 2020 ¹⁷		
11	Lu et al. 2020 ¹⁷	Lu et al. 2022 ¹⁸		
12	Lu et al. 2022 ¹⁸	Ninomiya et al. 2023 ²²		
13	Nair et al. 2021 ²⁰	Rios Velazquez et al. 2017 ²³		
14	Ninomiya et al. 2021 ²¹	Rossi et al. 2021 ²⁴		
15	RiosVelazquez et al. 2017 ²³	Tu et al. 2019 ²⁶		
16	Tu et al. 2019 ²⁶	Wang et al. 2022 ²⁷		
17	Wang et al. 2022 ²⁷	Weng et al. 2021 ²⁹		
18	Weng et al. 2021 ²⁹	Wu 2020 ³⁰		
19	Yang 2020 ³¹	Yang 2022 ³²		
20	Zhang 2020 ³⁴	Zhang 2018 ³³		

21	Zhang 2020 ³⁵	Zhang 2020 ³⁵		
22	Zhang 2021 ³⁶	Zhang 2021 ³⁶		
23	Zhao 2022 ³⁷	Zhu 2022 ³⁸		
24	Zhu 2022 ³⁸			

ALK, anaplastic lymphoma kinase; EGFR, epidermal growth factor receptor; KRAS, Kirsten rat sarcoma viral oncogene homologue.

Supplementary Table S4. Type of models (radiomic model/deep learning or combined [radiomic features + clinical variables]) developed in the studies for EGFR prediction and the radiomics/clinical features included. EGFR, epidermal growth factor receptor.

Study	Models	Radiomic features	Clinical variables
Chang et al. 2021 ¹	Radiomic	ShortRunLowGreyLevelEmphasis_AllDirection_offset1_SDH Percentile85 OneVoxelVolume Flatness ShortRunEmphasis_AllDirection_offset_SD HaralickCorrelation_AllDirection_offset4_SD Zone Percentage GLCM_Entropy_AllDirection_offset7_SD Correlation_AllDirection_offset7_SD CT_GLCMEntropy_AllDirection_offset1_SD HaralickCorrelation_angle135_offset7 LongRunHighGreyLevelEmphasis_angle0_offset ShortRunLowGreyLevelEmphasis_AllDirection_offset7_SD	N/A

		HaralickCorrelation_AllDirection_offset1_SD SurfaceVolumeRatio	
Dong et al. 2021 ³	Deep learning	Not specified	N/A
Dong et al. 2022 ⁴	Combined	wavelet-HLL_GLCM_MaximumProbability wavelet-LLL_GLCM_MaximumProbability original_GLCM_SumEntropy) log-sigma-1-0-mm-3D_GLCM_MaximumProbability wavelet-LHL_firstorder_Kurtosis wavelet-LLL_firstorder_Skewness log-sigma-2-0-mm-3D_firstorder_Kurtosis original_shape_Sphericity wavelet-LHL_GLSZM_LargeAreaHighG	Smoking status Histological type
Feng et al. 2022 ⁵	Radiomic	Skewness.7_firstorder_wavelet-LHL SmallAreaHighGrayLevelEmphasis.7_GLSZM_wavelet-LHL HighGrayLevelZoneEmphasis.12_GLSZM_wavelet-HHH 90Percentile_firstorder_original Variance.4_firstorder_square Range.4_firstorder_square	

		<p>GrayLevelVariance.26_GLSZM_wavelet-LHH</p> <p>JointAverage.11_GLCM_wavelet-HLH</p> <p>MeanAbsoluteDeviation.4_firstorder_square RobustMeanAbsoluteDeviation.4_firstorder_square</p> <p>GrayLevelNonUniformity.32_GLSZM_wavelet-LLH GrayLevelNonUniformity.1_girlm_original</p> <p>GrayLevelNonUniformity.4_girlm_logarithm GrayLevelNonUniformity.16_girlm_squareroot</p> <p>HighGrayLevelRunEmphasis.5_girlm_squareroot</p> <p>GrayLevelNonUniformityNormalized.21_GLSZM_wavelet-LLH LowGrayLevelRunEmphasis_girlm_original</p> <p>LowGrayLevelRunEmphasis.5_girlm_squareroot GrayLevelVariance.32_GLSZM_wavelet-LLH</p> <p>Minimum.4_firstorder_square SmallArealowGrayLevelEmphasis.11_GLSZM_wavelet-HLH</p> <p>SmallArealowGrayLevelEmphasis.12_GLSZM_wavelet-HHH</p> <p>Mean.12_firstorder_wavelet-HHH SmallArealowGrayLevelEmphasis.9_GLSZM_wavelet-HLL</p> <p>Imc2.12 GLCM wavelet-HHH</p> <p>ADC</p>	N/A
Gao et al. 2023 ⁶	Radiomic Combined	<p>original_firstorder_Kurtosis</p> <p>original_firstorder_Median</p> <p>original_firstorder_Skewness</p> <p>log-sigma-1-0-mm-3D_firstorder_Energy</p>	<p>CEA</p> <p>Sex (male)</p> <p>Nodule type (sub-</p>

		<p>log-sigma-4-0-mm-3D_GLDM_DependenceVariance</p> <p>wavelet-LHL_GLRLM_LongRunLowGrayLevelEmphasis</p> <p>wavelet-HLL_firstorder_Energy</p>	solidity)
Huo et al. 2022 ^{7*}	Combined	137 features (not specified)	<p>Age</p> <p>Sex (female)</p> <p>Non-smokers</p> <p>Clinical stage (I-II)</p>
Jia et al. 2019 ⁸	Combined	94 features (not specified)	<p>Sex</p> <p>Smoking history</p>
Jiang et al. 2022 ⁹	Combined	<p>Skewness</p> <p>Minimum</p> <p>Kurtosis</p> <p>Variance</p> <p>Minimum</p> <p>10th percentile</p>	<p>Age</p> <p>Sex</p>

		<p>SumSquare</p> <p>SizeZoneNonUniformity</p> <p>HighGrayLevelZoneEmphasis</p> <p>ZoneVariance</p> <p>LargeDependence HighGrayLevelEmphasis</p> <p>LargeDependenceHighGrayLevel Emphasis</p> <p>DependenceEntropy</p>	<p>Smoking</p> <p>Tumor</p> <p>Family history</p>
Le et al. 2021 ¹⁰	Radiomic	<p>wavelet-LLLfirstorderEnergy</p> <p>wavelet-LHHGLSZMGrayLevelNonUniformityNormalized</p> <p>wavelet-HHLGLDMSmallDependenceLowGratLevelEmphasis</p> <p>wavelet-HLHGLCM_MCC</p> <p>wavelet-HLHGLSZMSmallAreaLowGrayLevelEmphasis</p> <p>wavelet-HHHGLCMjointEnergy</p> <p>wavelet-HHHGLRLMGrayLevelNonUniformityNormalized</p>	N/A
Li et al. 2018 ¹¹	<p>Radiomic</p> <p>Combined</p>	338 features (not specified)	<p>Sex</p> <p>Smoking status</p>

Li et al. 2019 ¹²	Radiomic Combined	CT_GGS_Gray Span CT_GGC_Gray Mean	Age Sex Smoking status Clinical stage Lesion location
Li et al. 2020 ¹³	Combined	12 features (not specified)	Sex Age Smoking status
Li et al. 2022 ¹⁴	Radiomic	3 features (not specified)	–
Liu et al. 2020 ¹⁵	Radiomic Combined	RADIOMIC MODEL: wavelet-HLH_GLDM_DependenceVariance wavelet-LHL_GLDM_LargeDependenceLowGrayLevelEmphasis logarithm_GLCM_InverseVariance square_GLDM_DependenceVariance wavelet-HLH_GLDM_LargeDependenceHighGrayLevelEmphasis	

	<p>wavelet-HHH_GLCM_Id</p> <p>log-sigma-0-5-mm-3D_GLSZM_ZoneEntropy</p> <p>square_GLCM_Correlation</p> <p>original_GLCM_ClusterShade</p> <p>wavelet-LHH_GLDM_LargeDependenceHighGrayLevelEmphasis</p> <p>COMBINED MODEL:</p> <p>wavelet-HLH_GLDM_DependenceVariance</p> <p>custom_PatientSex</p> <p>logarithm_GLCM_InverseVariance</p> <p>square_GLCM_Correlation</p> <p>wavelet-HLL_firstorder_Kurtosis</p> <p>wavelet-LHL_GLRLM_LongRunLowGrayLevelEmphasis</p> <p>wavelet-HLL_firstorder_Median</p> <p>original_GLSZM_SizeZoneNonUniformityNormalized</p> <p>exponential_firstorder_Skewness</p>	<p>Age</p> <p>Sex</p> <p>Smoking history</p>
--	--	--

		wavelet-LLH_GLCM_ClusterShade	
Liu et al. 2022 ¹⁶	Radiomic	Mean absolute deviation 60 Percentile area Convex Correlation Dissimilarity 5-1 Homogeneity 2 10-4 Homogeneity 2 -333-7 Information measure corr 1 8-1 Information measure corr 1 9-7 Information measure corr 1 2-4 Inverse diff norm 6-4 Inverse variance 8-4 Inverse variance 8-1 Max Probability 12-7 Max Probability	-

		-333 Run length nonuniformity	
Lu et al. 2020 ¹⁷	Radiomic Combined	original_GLSZM_SmallAreaHighGrayLevelEmphasis original_GLSZM_SmallAreaLowGrayLevelEmphasis original_GLDM_LowGrayLevelEmphasis log-sigma-1-0-mm-3D_GLCM_Cluster Prominence log-sigma-3-0-mm-3D_GLDM_DependenceNonUniformityNormalized wavelet- LLL_GLCM_Inverse Variance wavelet-LLH_GLCM_Imc2 wavelet-HLL_firstorder_Mean wavelet-HLL_GLSZM_LowGrayLevelZoneEmphasis wavelet-HLL_GLDM_SmallDependenceHighGrayLevelEmphasis wavelet-HLH_GLSZM_SizeZoneNonUniformityNormalized wavelet-HHH_firstorder_Skewness wavelet-HHH_GLSZM_Size Zone Non Uniformity Normalized	Sex Smoking status Pathohistological subtype Vascular infiltration status
Lu et al. 2022 ¹⁸	Radiomic Combined	1269 features (not specified)	Age Sex Smoking status Stage of disease

			Serum level of tumor markers (CEA, CYFRA 21-1, SCC, Pro-GRP)
Nair et al. 2021 ^{20†}	Radiomic	NGTDM_600_Complexity G1rl_Saggital_30_ShortRunEmphasis G1rl_Saggital_30_ShortRunHighGrayLevelEmphasis G1rl_Saggital_120_ShortRunHighGrayLevelEmphasis G1rl_Coronal_120_ShortRunHighGrayLevelEmphasis G1rl_Coronal_30_ShortRunEmphasis G1rl_Saggital_120_ShortRunEmphasis G1rl_Axial_30_ShortRunEmphasis G1rl_Coronal_120_ShortRunEmphasis FirstOrder_HistogramBin2	-
Ninomiya et al. 2021 ²¹	Radiomic	BN MODEL: b0_GLCM_Energy_45, b1/b0_GLSZM_ZSN_104	

		<p>b1_GLCM_SumAverage_122</p> <p>b0_GLRLM_Lrlge_97)</p> <p>OI MODEL:</p> <p>GLRLM_ShortRunLowGrayLevelEmphasis</p> <p>GLSZM_LowGrayLevelZoneEmphasis</p> <p>GLSZM_ShortZoneLowGrayEmphasis</p> <p>WD MODEL:</p> <p>GLSZM_LowGrayLevelZoneEmphasis_LL</p>	-
Ninomiya et al. 2023 ²²	Combined	<p>GLSZM_SmallAreaLowGrayLevelEmphasis</p> <p>GLSZM_LargeAreaEmphasis</p> <p>Hist.RootMeanSquared</p> <p>GLDM_DependenceVariance</p>	Sex Smoking status
RiosVelazquez et al. 2017 ²³	Radiomic Combined	<p>imaging.Wavelet_LHH_GLCM_invDiffmomnor</p> <p>imaging.LoG_sigma_3_mm_3D_GLSZM_highIntensityLarteAreaEmp</p>	

	<p>First order_Root mean squared</p> <p>First order_Skewness</p> <p>First order_Uniformity</p> <p>GLCM_Correlation</p> <p>GLCM_Difference average</p> <p>GLCM_Difference entropy</p> <p>GLCM_InverseDifference</p> <p>GLCM_InverseDifferenceMoment</p> <p>GLCM_InverseDifferenceMomentNormalized</p> <p>GLCM_InverseDifferenceNormalized</p> <p>GLCM_InformationalMeasureCorrelation1</p> <p>GLCM_InformationalMeasureCorrelation2</p> <p>GLCM_InverseVariance</p> <p>GLCM_JointEnergy</p> <p>GLCM_JointEntropy</p> <p>GLCM_MaximalCorrelationCoefficient</p>	
--	---	--

		GLCM_MaximumProbability GLCM_SumEntropy GLDM_DependenceEntropy GLDM_DependenceNonUniformity GLDM_Dependence NonUniformityNormalized GLDM_DependenceVariance GLDM_GrayLevelNonUniformity GLDM_LargeDependenceEmphasis GLDM_SmallDependenceEmphasis GLRLM_GrayLevelNonUniformity GLRLM_GrayLevelNonUniformityNormalized GLRLM_RunEntropy GLRLM_RunPercentage GLRLM_ShortRunEmphasis GLSZM_GrayLevelNonUniformity GLSZM_GrayLevelNonUniformityNormalized	
--	--	--	--

		<p>GLSZM_SizeZoneNonUniformityNormalized</p> <p>GLSZM_SmallAreaEmphasis</p> <p>GLSZM_ZoneEntropy</p> <p>GLSZM_ZoneVariance</p> <p>NGTDM_Coarseness</p>	
Tu et al. 2019 ²⁶	<p>Radiomic</p> <p>Combined</p>	<p>X0_GLRLM_RunLengthNon-Uniformity</p> <p>X4_H_median</p> <p>X0_GLCM_homogeneity1</p>	<p>Maximum diameter</p> <p>Location</p> <p>Sex</p>
Wang et al. 2022 ²⁷	<p>Radiomic</p> <p>Combined[‡]</p>	Not specified	<p>Age</p> <p>Sex</p> <p>Tumor staging</p> <p>Number</p> <p>Size</p> <p>Past recurrence</p> <p>Medication status</p>

Weng et al. 2021 ²⁹	Combined	<p>SmallAreaEmphasis</p> <p>LongRunHigh GreyLevelEmphasis_angle0_offset4</p> <p>ClusterProminence_All Direction_offset7_SD</p> <p>InverseDifference Moment_All Direction_offset4_SD</p> <p>LowGreyLevel Run Emphasis_All Direction_offset4_SD</p> <p>LongRunLowGrey Level Emphasis_All Direction_offset7_SDCorrelation_angle0_offset7</p> <p>std Deviation</p> <p>GLCM Energy_All Direction_offset4_SD</p>	<p>Smoking status</p> <p>Spiculation</p> <p>Air bronchogram</p> <p>CEA</p> <p>SCCA</p>
Wu 2020 ³⁰	Combined	Not specified	<p>Smoking status</p> <p>Histological subtype</p>
Yang 2020 ³¹	Radiomic	Not specified	-
Yang 2022 ³²	<p>Radiomic</p> <p>Combined</p>	<p>Nonwavelet-LHH_NGTDMM_Strength</p> <p>wavelet-LHH_GLDM_DependenceEntropy</p> <p>wavelet-LLL_GLSZM_LargeAreaLowGrayLevelEmphasis</p> <p>wavelet-LLL_firstorder_Minimum</p>	<p>Sex</p> <p>Emphysema</p> <p>Interstitial lung disease</p>

		<p>wavelet-LLH_NGTDM_Contrast</p> <p>wavelet-LHH_NGTDM_Strength</p> <p>log-sigma-1-5-mm-3D_firstorder_Kurtosis</p> <p>wavelet-LHL_GLCM_ClusterShade</p> <p>wavelet-LHH_NGTDM_Strength</p> <p>wavelet-LLL_GLSZM_LargeAreaLowGrayLevelEmphasis</p> <p>wavelet-LLH_firstorder_Mean</p> <p>original_NGTDM_Contrast</p> <p>original_firstorder_Kurtosis</p> <p>log-sigma-1-5-mm-3D_firstorder_Kurtosis</p> <p>wavelet-LLL_NGTDM_Contrast</p> <p>original_GLCM_MaximumProbability</p> <p>wavelet-LLL_GLSZM_LargeAreaLowGrayLevelEmphasis</p>	
Zhang 2018 ³³	Combined	<p>IIF.range</p> <p>IIF.Skewness</p> <p>$W_{LLH}F.IF.mean_absulute_eviation$</p>	<p>Histological subtype</p> <p>Sex</p> <p>Smoking status</p>

		$W_{LHH}F.IF.median$ $W_{LLH}F.IF.mean$ $W_{LLH}F.GLCM.variance$ GLRLM_HighGrayLevelRunEmphasis	
Zhang 2020 ³⁴	Radiomic	GLSZM_HighGrayLevelZoneEmphasis GLDM_DependenceVariance GLSZM_GreyLevelNon UniformityNormalized GLSZM_ZoneEntropy	-
Zhang 2020 ³⁵	Radiomic Combined	784 features (not specified)	Sex Histopathological Subtype Age
Zhang 2021 ³⁶	Radiomic Combined	fo_Skewness exp_GLRLM_ShortRunEmphasis exp_GLRLM_ShortRunHighGrayLevelEmphasis exp_GLDM_SmallDependenceEmphasis	Smoking history Bubble-like lucency Pleural attachment Pleural retraction

		grad_GLDM_DependenceEntropy LLH_fo_90P LLH_GLCM_SumEntropy LLL-fo_kurtosis LLL-GLCM_ClusterProminence LLL_GLSZM_GrayLevelNonUniformityNormalized LLL_GLSZM_GrayLevelVariance LLL_GLSZM_ZoneEntropy	
Zhao 2022 ^{37§}	Radiomic	CT_Shape_Sphericity CT_GLRLM_ShortRunEmphasis CT_GLRLM_ShortRunHighGreyLevelEmphasis CT_NGLDM_Busyness CT_Glzlm_ShortZoneEmphasis	-
Zhu 2022 ³⁸	Radiomic Combined	log_sigma_1.0_mm_3D_GLRLM_RunVariance wavelet_LLH_firstorder_RootMeanSquared log-sigma-2-0-mm-3D_GLCM_ClusterShade	Sex Age Emphysema

	wavelet_HHH_firstorder_Mean	Pathological subtype
--	-----------------------------	----------------------

*Combined model also included 14 CT features: location (peripheral), tumor size ≥ 3 cm, subsolid density, spiculation, lobulation, air bronchogram, air space, necrosis, calcification (presence), vascular convergence sign, pleural retraction sign, pleural effusion, lymphatic metastasis and multiple pulmonary metastasis.

†Top 10 selected features. The maximum number of texture features included was determined by maximizing cross-validated accuracy. This value was not the same for each binary group or each machine learning model.

‡Note that this model includes radiomic features + deep features and clinical variables.

§Model 1.

BN, Betti numbers; CEA, carcinoembryonic antigen; CYFRA 21-1, fragment of cytokeratin sub-unit 19; GLCM, gray-level co-occurrence matrix; GLDM, gray-level dependence matrix; GLRLM, gray-level run-length matrix; GLSZM, gray-level size zone matrix; NGTDM, neighbouring gray tone difference matrix; OI, original image; Pro-GRP, pro-gastrin-releasing peptide; SCC, squamous cell carcinoma antigen; WD, wavelet decomposition.

Supplementary Table S5. Type of models (radiomic model or combined [radiomic features + clinical variables]) developed in the studies for ALK prediction and the radiomics/clinical features included. ALK, anaplastic lymphoma kinase.

Study	Models	Radiomic features	Clinical variables
Chang et al. 2021 ²	Radiomic	CT_uniformity CT_LongRunEmphasis_AllDirection_offset4_SD CT_HaraEntropy CT_GLCMEnergy_angle135_offset7 CT_LongRunHighGreyLevelEmphasis_angle45_offset1 CT_LongRunLowGreyLevelEmphasis_AllDirection_offset7_SD CT_Correlation_AllDirection_offset4_SD CT_Percentile70 CT_HaralickCorreltion_AllDirection_offset4_SD CT_LongRunLowGreyLevelEmphasis_AllDirection_offset4_SD CT_LongRunEmphasis_angle135_offset4 CT_LongRunHighGreyLevelEmphasis_angle90_offset4	-

		<p>CT_LongRunLowGreyLevelEmphasis_AllDirection_offset1_SD</p> <p>CT_HaralickCorreltion_AllDirection_offset7_SD</p> <p>CT_ShortRunEmphasis_AllDirection_offset1_SD</p> <p>CT_LongRunHighGreyLevelEmphasis_angle0_offset1</p> <p>CT_GLCMEntropy_angle90_offset1</p> <p>CT_Percentile30</p> <p>CT_LongRunEmphasis_angle90_offset4</p> <p>CT_LongRunEmphasis_AllDirection_offset1_SD</p>	
Ma et al. 2020 ¹⁹	Radiomic	<p>PRE-CONTRAST MODEL:</p> <p>wavelet-LLL_GLCM_DifferenceVariance</p> <p>wavelet-LLH_firstorder_Median</p> <p>wavelet-LLH_NGTDN_Busyness</p> <p>wavelet-LHL_GLSZM_LargeAreaLowGrayLevelEmphasis</p> <p>wavelet-HHH_GLSZM_LargeAreaLowGrayLevelEmphasis</p> <p>wavelet-LHL_firstorder_Energy</p>	-

		<p>wavelet-HHL_firstorder_90Percentile</p> <p>wavelet-HHL_GLCM_JointEntropy</p> <p>wavelet-HHL_firstorder_Uniformity</p> <p>wavelet-HHL_firstorder_RobustMeanAbsoluteDeviation</p> <p>wavelet-LHH_GLDM_LargeDependenceLowGrayLevelEmphasis</p> <p>wavelet-HLH_firstorder_Median</p> <p>wavelet-LHL_GLDM_LargeDependenceLowGrayLevelEmphasis</p> <p>wavelet-HHL_GLCM_InverseDifference</p> <p>wavelet-HHL_firstorder_InterquartileRange</p> <p>wavelet-HHL_GLCM_MaximumProbabilility</p> <p>wavelet-HHH_GLSZM_SmallAreaLowGrayLevelEmphasis</p> <p>wavelet-HHL_firstorder_Mean</p> <p>wavelet-HLL_GLCM_ClusterShade</p> <p>wavelet-HHL_GLSZM_SmallAreaLowGrayLevelEmphasis</p> <p>wavelet-LHH_GLCM_MaximalCorrelationCoefficient</p> <p>wavelet-LLL_GLSZM_SizeZoneNonUniformityNormalized</p>	
--	--	--	--

		<p>wavelet-LLL_GLSZM_SmallAreaEmphasis</p> <p>wavelet-HHL_GLCM_InverseDifferenceNormalized</p> <p>POST-CONTRAST MODEL:</p> <p>wavelet-LHH_GLDM_SmallDependenceHighGrayLevelEmphasis</p> <p>wavelet_HHL_GLSZM_GrayLevelNonUniformity</p> <p>wavelet-LLH_firstorder_Mean</p> <p>wavelet-LLH_GLSZM_HighGrayLevelZoneEmphasis</p> <p>wavelet-LLH_GLSZM_SmallAreaHighGrayLevelEmphasis</p> <p>wavelet-LLH_GLSZM_SmallAreaLowGrayLevelEmphasis</p> <p>wavelet-HHH_GLCM_MaximumProbability</p> <p>wavelet-LLL_GLDM_LargeDependenceLowGrayLevelEmphasis</p> <p>wavelet-HLL_GLDM_DependenceVariance</p> <p>wavelet-HHH_firstorder_Mean</p> <p>wavelet-HHH_GLDM_LowGrayLevelEmphasis</p> <p>wavelet-LLH_firstorder_90Percentile</p>	
--	--	--	--

		wavelet-HHL_GLDM_DependenceVariance wavelet-HHH_GLCM_MaximalCorrelationCoefficient wavelet-HHH_NGTDm_Contrast wavelet-original_GLCM_InverseVariance wavelet-LLH_firstorder_Range wavelet-HHL_GLCM_MaximalCorrelationCoefficient wavelet-HLL_GLSZM_GrayLevelNonUniformityNormalized	
Song et al. 2020 ²⁵	Radiomic Combined	RADIOMIC MODEL: Original_Firstorder_90Percentile Original_Firstorder_Entropy Original_Firstorder_Maximum Wavelet-LHH_Firstorder_10Percentile Wavelet-HLL_Firstorder_Median Wavelet-HHH_Firstorder_Mean LoG-sigma-1-0-mm-3D_Firstorder_Median	Age Sex Smoking history

		<p>LoG-sigma-1-0-mm-3D_Firstorder_RootMeanSquared</p> <p>LoG-sigma-1-0-mm-3D_Firstorder_Minimum</p> <p>LoG-sigma-2-0-mm-3D_Firstorder_10Percentile</p> <p>LoG-sigma-3-0-mm-3D_Firstorder_90Percentile</p> <p>LoG-sigma-5-0-mm-3D_Firstorder_Skewness</p> <p>Original_GLCM_ClusterShade</p> <p>Wavelet-LHH_GLCM_Correlation</p> <p>Wavelet-LHL_GLCM_InverseDifferenceNormalized</p> <p>Wavelet-HHH_GLCM_InformationalMeasureofCorrelation1</p> <p>LoG-sigma-1-0-mm-3D_GLCM_Autocorrelation</p> <p>LoG-sigma-2-0-mm-3D_GLCM_InverseVariance</p> <p>Original_GLSZM_SmallAreaHighGrayLevelEmphasis</p> <p>Wavelet-HHH_GLSZM_SmallAreaHighGrayLevelEmphasis</p> <p>Wavelet-HLL_GLSZM_ZoneEntropy</p> <p>Wavelet-HLH_GLSZM_ZoneEntropy</p> <p>LoG-sigma-2-0-mm-3D_GLSZM_ZoneEntropy</p>	<p>Smoking index</p> <p>Clinical stage Distal metastasis</p> <p>Pathological invasiveness of the tumor</p>
--	--	---	--

		<p>LoG-sigma-3-0-mm-3D_GLSZM _ SmallAreaEmphasis</p> <p>LoG-sigma-3-0-mm-3D_GLSZM _ Size-ZoneNonUniformityNormalized</p> <p>LoG-sigma-5-0-mm-3D_GLSZM _ GrayLevelNonUniformityNormalized</p> <p>Wavelet-LHH_GLDM_ LargeDependenceHighGrayLevelEmphasis</p> <p>LoG-sigma-1-0-mm-3D_GLDM _ HighGrayLevelEmphasis</p> <p>LoG-sigma-3-0-mm-3D_GLRLM_RunPercentage</p> <p>LoG-sigma-4-0-mm-3D_GLRLM _ LongRunLowGrayLevelEmphasis</p> <p>COMBINED MODEL:</p> <p>Current smoker</p> <p>Stage I</p> <p>Male</p> <p>Local lymphadenopathy</p> <p>Pericardial effusion</p> <p>Left Lower Lobe lesion</p> <p>No cavity in the lesion</p>	
--	--	---	--

		<p>Lobulated margin</p> <p>No pleural retraction sign</p> <p>No local lymphadenopathy</p> <p>Wavelet-HHL_Firstorder_Kurtosis</p> <p>Wavelet-HLL_Firstorder_Median</p> <p>Wavelet-LHH_Firstorder_Skewness</p> <p>Wavelet-LLL_Firstorder_Minimum</p> <p>Wavelet-HLH_Firstorder_Median</p> <p>LoG-sigma-1-0-mm-3D_Firstorder_Minimum</p> <p>LoG-sigma-2-0-mm-3D_Firstorder_Minimum</p> <p>Wavelet-LLL_GLCM_ClusterShade</p> <p>Wavelet-LLH_GLCM _InformationalMeasureofCorrelation2</p> <p>Wavelet-HLH_GLCM _InformationalMeasureofCorrelation2</p> <p>Wavelet-HLH_GLCM _InformationalMeasureofCorrelation1</p> <p>LoG-sigma-1-0-mm-3D_GLCM _InformationalMeasureofCorrelation1</p> <p>LoG-sigma-3-0-mm-3D_GLCM _InformationalMeasureofCorrelation2</p>	
--	--	--	--

		LoG-sigma-5-0-mm-3D_GLCM_InformationalMeasureofCorrelation2 Original_Shape_MajorAxisLength Wavelet-HLH_GLSZM_SizeZoneNon-Uniformity LoG-sigma-4-0-mm-3D_GLSZM_GrayLevelNonUniformityNormalized Wavelet-HLH_GLDM_ LargeDependenceHigh GrayLevelEmphasis Wavelet-HHH_GLDM_ LargeDependenceHigh GrayLevelEmphasis Original_GLRLM_ HighGrayLevelRunEmphasis	
--	--	---	--

GLCM , gray-level co-occurrence matrix; GLDM , gray-level dependence matrix; GLRLM , gray-level run-length matrix; GLSZM , gray-level size zone matrix; NGTDM , neighbouring gray tone difference matrix.

Supplementary Table S6. Type of models (radiomic model or combined [radiomic features + clinical variables]) developed in the studies for KRAS prediction and the radiomics/clinical features included. KRAS, Kirsten rat sarcoma viral oncogene homologue.

Study	Models	Radiomic features	Clinical variables
Dong et al. 2021 ³	Radiomic	Not specified	-
Le et al. 2021 ¹⁰	Radiomic	wavelet-LLHGLSZMLargeAreaEmphasis wavelet-LLLGLDMDependenceEntropy wavelet-LHHGLDMLargeDependenceLowGrayLevelEmphasis ori-firstorderkurtosis wavelet-HLHGLCMInverseVariance wavelet-HLLGLSZMSmallAreaHighGrayLevelEmphasis wavelet-LHHGLCMId wavelet-HHLGLCMDifferenceEntropy	-

		<p>wavelet-LLLGLSZMGrayLevelNonUniformityNormalized</p> <p>wavelet-HHHGLCMDifferenceAverage</p> <p>wavelet-HHHGLDMDependenceEntropy</p>	
RiosVelazquez et al. 2017 ²³	<p>Radiomic</p> <p>Combined</p>	<p>imaging.LoG_sigma_3_mm_3D_GLSZM_highIntensityLarteAreaEmp</p> <p>imaging.Wavelet_LHH_GLCM_clusProm imaging.Wavelet_LHH_GLCM_energy</p> <p>imaging.Wavelet_LLL_stats_energy imaging.Wavelet_LLL_stats_median</p> <p>imaging.LoG_sigma_3_mm_3D_GLSZM_largeAreaEmphasis</p> <p>imaging.Wavelet_HHH_GLSZM_lowIntensitySmallAreaEmp</p> <p>imaging.Wavelet_HHH_GLCM_correl1 imaging.LoG_sigma_3_mm_3D_GLCM_clusProm</p> <p>imaging.Wavelet_LLL_GLSZM_highIntensityLarteAreaEmp imaging.Wavelet_HHL_stats_energy</p> <p>imaging.Wavelet_HLL_stats_var imaging.Wavelet_HLH_GLSZM_lowIntensitySmallAreaEmp</p> <p>imaging.Wavelet_LHH_rlgl_GrayLevelNonuniformity</p> <p>imaging.LoG_sigma_3_mm_3D_GLSZM_lowIntensitySmallAreaEmp imaging.GLCM_clusShade</p> <p>imaging.Wavelet_LHH_GLCM_invDiffmomnor imaging.Wavelet_HLL_stats_min</p> <p>imaging.Wavelet_LLL_rlgl_longRunHighGrayLevEmpha imaging.Wavelet_LLH_stats_mean</p>	<p>Stage</p> <p>Sex</p> <p>Smoking status</p> <p>Age</p> <p>Race</p>
Wang et al. 2022 ²⁸	Radiomic	<p>CT_square_GLSZM_SizeZoneNonUniformityNormalized</p> <p>CT_wavelet-LHH_GLDM_DependenceNonUniformityNormalized</p>	-

		CT_wavelet-HHL_firstorder_Skewness	
		CT_wavelet-HHL_GLDM_DependenceNonUniformityNormalized	

GLCM , gray-level co-occurrence matrix; GLDM , gray-level dependence matrix; GLRLM , gray-level run-length matrix; GLSZM , gray-level size zone matrix.

Supplementary Table S7. Results of the meta-regression analyzing the effects of age, type of segmentation (manual/semi-automatic/automatic), type of model (radiomics/combined [radiomic features + clinical data] and artificial intelligence methodology (machine learning/deep learning).

AGE					
Fixed-effects coefficients					
	Estimate	SE	z	p-value	CI 95%
tsens.(Intercept)	4.488	2.181	2.058	0.040	[0.214, 8.762]
tsens.AGE	-0.052	0.035	-1.483	0.138	[-0.121, 0.017]
tfpr.(Intercept)	-0.156	2.288	-0.068	0.946	[-4.640, 4.328]
tfpr.AGE	-0.012	0.037	-0.318	0.750	[-0.084, 0.061]
Variance components: between-studies Std. Dev and correlation matrix					
	SD	tsens		tfpr	
tsens	0.395	-		0.819	
tfpr	0.431	0.819		-	
TYPE OF SEGMENTATION					
Fixed-effects coefficients					
	Estimate	SE	z	p-value	CI 95%
tsens.(Intercept)	1.217	0.127	9.599	0.000	[0.968, 1.465]
tsens.SegmentationSemiautomatic	-0.086	0.241	-0.356	0.722	[-0.558, 0.387]

tsens.SegmentationUnknown	0.347	0.708	0.491	0.624	[-1.040, 1.734]
tfpr.(Intercept)	-0.984	0.133	-7.426	0.000	[-1.244, -0.725]
tfpr.SegmentationSemiautomatic	0.272	0.254	1.067	0.286	[-0.227, 0.770]
tfpr.SegmentationUnknown	0.397	0.697	0.569	0.569	[-0.970, 1.763]
Variance components: between-studies Std. Dev and correlation matrix					
	SD		tsens		tfpr
tsens	0.465		-		0.827
tfpr	0.511		0.827		-
CONTRAST					
Fixed-effects coefficients					
	Estimate	SE	z	p-value	CI 95%
tsens.(Intercept)	1.244	0.608	2.045	0.041	[0.052, 2.437]
tsens.Contrastcontrast-enhanced	0.151	0.650	0.232	0.817	[-1.124, 1.425]
tsens.Contrastnon-contrast CT	-0.096	0.620	-0.156	0.876	[-1.312, 1.119]
tfpr.(Intercept)	-0.619	0.638	-0.970	0.332	[-1.870, 0.632]
tfpr.Contrastcontrast-enhanced	-0.509	0.683	-0.745	0.456	[-1.848, 0.829]
tfpr.Contrastnon-contrast CT	-0.309	0.650	-0.476	0.634	[-1.584, 0.965]
Variance components: between-studies Std. Dev and correlation matrix					

	SD	tsens	tfpr		
tsens	0.468	-	0.889		
tfpr	0.511	0.889	-		
TYPE OF MODEL					
Fixed-effects coefficients					
	Estimate	SE	z	p-value	CI 95%
tsens.(Intercept)	1.281	0.133	9.603	0.000	[1.020, 1.543]
tsens.Modelrad	-0.193	0.197	-0.980	0.327	[-0.579, 0.193]
tfpr.(Intercept)	-0.939	0.146	-6.413	0.000	[-1.226, -0.652]
tfpr.Modelrad	0.006	0.222	0.026	0.979	[-0.429, 0.441]
Variance components: between-studies Std. Dev and correlation matrix					
	SD	tsens	tfpr		
tsens	0.434	-	0.828		
tfpr	0.524	0.828	-		
AI METHODOLOGY					
Fixed-effects coefficients					
	Estimate	SE	z	p-value	CI 95%
tsens.(Intercept)	1.215	0.232	5.2240	0.000	[0.761, 1.670]
tsens.TypeML	-0.022	0.257	-0.087	0.930	[-0.526, 0.481]

tfpr.(Intercept)	-0.898	0.257	-3.489	0.000	[-1.403, 0.394]
tfpr.TypeML	-0.052	0.285	-0.184	0.854	[-0.610, 0.505]
Variance components: between-studies Std. Dev and correlation matrix					
	SD	tsens	tfpr		
tsens	0.442	-	0.795		
tfpr	0.520	0.795	-		

AI, artificial intelligence; CI, confidence interval; ML, machine learning; rad, model including only radiomic features; SE, standard error; SD, Standard deviation; z, standard score in a gaussian distribution; tsens, logarithmic transformation of sensitivity; tfpr, logarithmic transformation of false positive rate.

REFERENCES

- 1 Chang C, Zhou S, Yu H et al. A clinically practical radiomics-clinical combined model based on PET/CT data and nomogram predicts EGFR mutation in lung adenocarcinoma. *Eur Radiol*. 2021; 31(8): 6259-6268.
- 2 Chang C, Sun X, Wang G et al. A machine learning model based on PET/CT radiomics and clinical characteristics predicts ALK rearrangement status in lung adenocarcinoma. *Front Oncol*. 2021; 11: 603882.
- 3 Dong Y, Hou L, Yang W et al. Multi-channel multi-task deep learning for predicting EGFR and KRAS mutations of non-small cell lung cancer on CT images. *Quant Imaging Med Surg*. 2021; 11(6): 2354-2375.
- 4 Dong Y, Jiang Z, Li C et al. Development and validation of novel radiomics-based nomograms for the prediction of EGFR mutations and Ki-67 proliferation index in non-small cell lung cancer. *Quant Imaging Med Surg*. 2022; 12(5): 2658-2671.
- 5 Feng Y, Song F, Zhang P et al. Prediction of EGFR mutation status in non-small cell lung cancer based on ensemble learning. *Front Pharmacol*. 2022; 13: 897597.
- 6 Gao J, Niu R, Shi Y et al. The predictive value of [(18)F]FDG PET/CT radiomics combined with clinical features for EGFR mutation status in different clinical staging of lung adenocarcinoma. *EJNMMI Res*. 2023; 13(1): 26.
- 7 Huo JW, Luo TY, Diao L et al. Using combined CT-clinical radiomics models to identify epidermal growth factor receptor mutation subtypes in lung adenocarcinoma. *Front Oncol*. 2022; 12: 846589.
- 8 Jia TY, Xiong JF, Li XY et al. Identifying EGFR mutations in lung adenocarcinoma by noninvasive imaging using radiomics features and random forest modeling. *Eur Radiol*. 2019; 29(9): 4742-4750.
- 9 Jiang M, Yang P, Li J et al. Computed tomography-based radiomics quantification predicts epidermal growth factor receptor mutation status and

- efficacy of first-line targeted therapy in lung adenocarcinoma. *Front Oncol.* 2022; 12: 985284.
- 10 Le NQK, Kha QH, Nguyen VH et al. Machine learning-based radiomics signatures for EGFR and KRAS mutations prediction in non-small-cell lung cancer. *Int J Mol Sci.* 2021; 22(17).
 - 11 Li XY, Xiong JF, Jia TY et al. Detection of epithelial growth factor receptor (EGFR) mutations on CT images of patients with lung adenocarcinoma using radiomics and/or multi-level residual convolutionary neural networks. *J Thorac Dis.* 2018; 10(12): 6624-6635.
 - 12 Li X, Yin G, Zhang Y et al. Predictive power of a radiomic signature based on (18)F-FDG PET/CT images for EGFR mutational status in NSCLC. *Front Oncol.* 2019; 9: 1062.
 - 13 Li S, Luo T, Ding C et al. Detailed identification of epidermal growth factor receptor mutations in lung adenocarcinoma: Combining radiomics with machine learning. *Med Phys.* 2020; 47(8): 3458-3466.
 - 14 Li S, Li Y, Zhao M et al. Combination of (18)F-fluorodeoxyglucose PET/CT radiomics and clinical features for predicting epidermal growth factor receptor mutations in lung adenocarcinoma. *Korean J Radiol.* 2022; 23(9): 921-930.
 - 15 Liu G, Xu Z, Ge Y et al. 3D radiomics predicts EGFR mutation, exon-19 deletion and exon-21 L858R mutation in lung adenocarcinoma. *Transl Lung Cancer Res.* 2020; 9(4): 1212-1224.
 - 16 Liu Y, Zhou J, Wu J et al. Development and validation of machine learning models to predict epidermal growth factor receptor mutation in non-small cell lung cancer: a multi-center retrospective radiomics study. *Cancer Control.* 2022; 29: 10732748221092926.
 - 17 Lu X, Li M, Zhang H et al. A novel radiomic nomogram for predicting epidermal growth factor receptor mutation in peripheral lung adenocarcinoma. *Phys Med Biol.* 2020; 65(5): 055012.

- 18 Lu J, Ji X, Wang L et al. Machine learning-based radiomics for prediction of epidermal growth factor receptor mutations in lung adenocarcinoma. *Dis Markers*. 2022; 2022: 2056837.
- 19 Ma DN, Gao XY, Dan YB et al. Evaluating solid lung adenocarcinoma anaplastic lymphoma kinase gene rearrangement using noninvasive radiomics biomarkers. *Onco Targets Ther*. 2020; 13: 6927-6935.
- 20 Nair JKR, Saeed UA, McDougall CC et al. Radiogenomic models using machine learning techniques to predict EGFR mutations in non-small cell lung cancer. *Can Assoc Radiol J*. 2021; 72(1): 109-119.
- 21 Ninomiya K, Arimura H, Chan WY et al. Robust radiogenomics approach to the identification of EGFR mutations among patients with NSCLC from three different countries using topologically invariant Betti numbers. *PLoS One*. 2021; 16(1): e0244354.
- 22 Ninomiya K, Arimura H, Tanaka K et al. Three-dimensional topological radiogenomics of epidermal growth factor receptor Del19 and L858R mutation subtypes on computed tomography images of lung cancer patients. *Comput Methods Programs Biomed*. 2023; 236: 107544.
- 23 Rios Velazquez E, Parmar C, Liu Y et al. Somatic mutations drive distinct imaging phenotypes in lung cancer. *Cancer Res*. 2017; 77(14): 3922-3930.
- 24 Rossi G, Barabino E, Fedeli A et al. Radiomic detection of EGFR mutations in NSCLC. *Cancer Res*. 2021; 81(3): 724-731.
- 25 Song L, Zhu Z, Mao L et al. Clinical, conventional ct and radiomic feature-based machine learning models for predicting ALK rearrangement status in lung adenocarcinoma patients. *Front Oncol*. 2020; 10: 369.
- 26 Tu W, Sun G, Fan L et al. Radiomics signature: A potential and incremental predictor for EGFR mutation status in NSCLC patients, comparison with CT morphology. *Lung Cancer*. 2019; 132: 28-35.
- 27 Wang C, Ma J, Shao J et al. Predicting EGFR and PD-L1 status in NSCLC patients using multitask ai system based on CT images. *Front Immunol*. 2022; 13: 813072.

- 28 Wang J, Lv X, Huang W et al. Establishment and optimization of radiomics algorithms for prediction of KRAS gene mutation by integration of NSCLC gene mutation mutual exclusion information. *Front Pharmacol.* 2022; 13: 862581.
- 29 Weng Q, Hui J, Wang H et al. Radiomic feature-based nomogram: a novel technique to predict EGFR-activating mutations for EGFR tyrosin kinase inhibitor therapy. *Front Oncol.* 2021; 11: 590937.
- 30 Wu S, Shen G, Mao J et al. CT radiomics in predicting EGFR mutation in non-small cell lung cancer: a single institutional study. *Front Oncol.* 2020; 10: 542957.
- 31 Yang C, Chen W, Gong G et al. Application of CT radiomics features to predict the EGFR mutation status and therapeutic sensitivity to TKIs of advanced lung adenocarcinoma. *Transl Cancer Res.* 2020; 9(11): 6683-6690.
- 32 Yang X, Liu M, Ren Y et al. Using contrast-enhanced CT and non-contrast-enhanced CT to predict EGFR mutation status in NSCLC patients-a radiomics nomogram analysis. *Eur Radiol.* 2022; 32(4): 2693-2703.
- 33 Zhang L, Chen B, Liu X et al. Quantitative biomarkers for prediction of epidermal growth factor receptor mutation in non-small cell lung cancer. *Transl Oncol.* 2018; 11(1): 94-101.
- 34 Zhang M, Bao Y, Rui W et al. Performance of (18)F-FDG PET/CT radiomics for predicting EGFR mutation status in patients with non-small cell lung cancer. *Front Oncol.* 2020; 10: 568857.
- 35 Zhang B, Qi S, Pan X et al. Deep CNN model using CT radiomics feature mapping recognizes EGFR gene mutation status of lung adenocarcinoma. *Front Oncol.* 2020; 10: 598721.
- 36 Zhang G, Cao Y, Zhang J et al. Predicting EGFR mutation status in lung adenocarcinoma: development and validation of a computed tomography-based radiomics signature. *Am J Cancer Res.* 2021; 11(2): 546-560.

- 37 Zhao HY, Su YX, Zhang LH et al. Prediction model based on 18F-FDG PET/CT radiomic features and clinical factors of EGFR mutations in lung adenocarcinoma. *Neoplasma*. 2022; 69(1): 233-241.
- 38 Zhu H, Song Y, Huang Z et al. Accurate prediction of epidermal growth factor receptor mutation status in early-stage lung adenocarcinoma, using radiomics and clinical features. *Asia Pac J Clin Oncol*. 2022; 18(6): 586-594.